의학박사 학위논문

The role of SNX18 in modulating endocytic trafficking and deleterious effect of Aβ oligomers in synaptic vesicle trafficking

세포내 수송과정에서 SNX18의 역할과 시냅스낭 순환과정에서의 Aβ oligomers의 유해한 효과에 관한 연구

2013년 2월

서울대학교 대학원

의과학과 의과학전공

박 주 현

A thesis of the Degree of Doctor of Philosophy

세포내 수송과정에서 SNX18의 역할과 시냅스낭 순환과정에서의 Aβ oligomers의 유해한 효과에 관한 연구

The role of SNX18 in modulating endocytic trafficking and deleterious effect of Aβ oligomers in synaptic vesicle trafficking

February 2013

The Department of Biomedical Sciences

Seoul National University

College of Medicine

Joohyun Park

ABSTRACT

The role of SNX18 in modulating endocytic trafficking and deleterious effect of Aβ oligomers in synaptic vesicle trafficking

Joohyun Park

Department of Biomedical Sciences

The Graduate School

Seoul National University

SNX18 and SNX9 are members of a subfamily of sorting nexin (SNX) proteins with the same domain structure. Although a recent report showed that SNX18 and SNX9 localize differently in cells and appear to function in different trafficking pathways, concrete evidence regarding whether they act together or separately in intracellular trafficking is still lacking. Here, I found that SNX18 has a similar role to SNX9 in endocytic trafficking at the plasma membrane, rather than having a distinct role. SNX18 and SNX9 are expressed

together in most cell lines, but to a different extent. Like SNX9, SNX18 interacts with dynamin and stimulates the basal GTPase activity of dynamin. It also interacts with neuronal Wiskott-Aldrich syndrome protein (N-WASP) and synaptojanin, as does SNX9. SNX18 and SNX9 can form a heterodimer and colocalize in tubular membrane structures. Depletion of SNX18 by small hairpin RNA inhibits transferrin uptake. SNX18 successfully compensates for SNX9 deficiency during clathrin-mediated endocytosis and vice versa. Total internal reflection fluorescence microscopy in living cells shows that a transient burst of SNX18 recruitment to clathrin-coated pits coincides spatiotemporally with a burst of dynamin and SNX9. Taken together, these results are suggested that SNX18 functions with SNX9 in multiple pathways of endocytosis at the plasma membrane and that they are functionally redundant.

The second part of my dissertation, I studied the effects of soluble Aβ oligomers in the synaptic vesicle (SV) trafficking. Aβ oligomers are known to be correlated well with many early aspects of Alzheimer's disease (AD) pathogenesis. Although considerable evidence supports the link between Aβ oligomers and postsynaptic dysfunction, the effects of Aβ oligomers in presynaptic function continue to be revealed. The current study demonstrated that acute treatment with nanomolar concentration of Aβ oligomers results in a decrease of the recycling pool while the resting vesicle pool increases concomitantly in cultured hippocampal neurons. SV endocytosis and the regeneration of fusion-competent vesicle are also severely impaired. Furthermore, the release probability of the readily-releasable pool (RRP) is

increased and the recovery rate after depletion of RRP is significantly delayed. All deficits are prevented by the antibody against Aβ, 6E10. The synaptojanin expression level is increased by Aβ oligomers, but Ca^{2+} clearance rate is not affected. The endocytic deficits by Aβ oligomers are fully restored by phosphatidylinositol-4-phosphate-5-kinase type I-γ expression while pool size alteration is recovered by inhibition of calpain-CDK5-mediated pathway, suggesting that two distinct downstream pathways involves in Aβ oligomers-induced presynaptic dysfunction. Together, my results suggest that Aβ oligomers cause defects in multiple steps of SV trafficking via different downstream pathways, which may affect presynaptic efficacy leading to synaptic dysfunction associated with AD.

* This work is published in *J Cell Sci.* Journal (Park J, Kim Y, Lee S, Park JJ, Park ZY, Sun W. et al. SNX18 shares a redundant role with SNX9 and modulates endocytic trafficking at the plasma membrane. *J Cell Sci.* 2010;123(Pt 10):1742-50.).

Keywords : SNX18, SNX9, CME, dynamin, membrane tubulation, Alzheimer's disease, soluble Aβ oligomers, synaptic dysfunction, presynaptic function, synaptic vesicle (SV) trafficking, phosphatidylinositol-4,5-bisphosphate (PIP_2), cyclin-dependent kinase 5 (CDK5)

Student Number : 2009-30603

CONTENTS

LIST OF FIGURES

<CHAPTER 1>

<CHAPTER 2>

LIST OF ABBREVIATIONS

SNXs, Sorting nexins

SH3, Src homology 3

BAR, Bin–Amphiphysin–Rvs

PRD, Proline-rich domain

N-WASP, Neuronal Wiskott-Aldrich syndrome protein

CME, Clathrin-mediated endocytosis

CCP, Clathrin-coated pit

TIRF-M, Total internal reflection fluorescence microscopy

AP-1, Adaptor protein complex 1

CI-MPR, Cation-independent mannose-6-phosphate receptor

AD, Alzheimer's disease

PIP2, Phosphatidylinositol-4,5-bisphosphate

PIPkinase-γ, Phosphatidylinositol-4-phosphate-5-kinase type I-γ

CDK5, Cyclin-dependent kinase 5

CI, Calpain inhibitor

APs, Action potentials

RRP, Readily-releasable pool

RP, Recycling pool

Pr, Release probability

SV, Synaptic vesicle

GENERAL INTRODUCTION

Endocytosis is a key process for non-neuronal cells and neuronal cells to interact with their environment. Among various endocytic processes, clathrin-mediated endocytosis (CME) is most well-studied. During CME, many adaptors and accessory proteins, such as AP-2, AP-180, clathrin and synaptotagmin, are recruited to phosphatidylinositol 4,5-bisphosphate (PIP_2)-enriched plasma membrane for coat nucleation and assembly (1). These are followed by membrane invagination that involves the coordinated actions by other endocytic proteins such as actin, synaptojanin, endophilin and amphiphysin for maturation of clathrin-coated pit (CCP) (2-3). Subsequently, dynamin, a GTPase protein, is recruited to the neck of the membrane invagination to separate CCP from the plasma membrane (4-10). Finally, the endocytosed vesicles are uncoated by auxilin, hsc70 and synaptojanin, and freed clathrin, AP-2 and AP-180 are reused for the next round of CME (11).

CME also occurs in the presynaptic terminal of neurons, but the exact process of synaptic vesicle (SV) endocytosis still remains much more to be revealed. The basal mechanisms and related proteins in CME, however, are expected to be similar between non-neuronal cells and neuronal cells, although some proteins such as stonin 2, Eps15 and intersectin are found to be exclusively expressed in the neurons (12-13).

SNX9 (sorting nexin 9) plays a critical role in CME by interacting with N-WASP, synaptojanin and dynamin. In addition, as a Bin-Amphiphysin-Rvs

(BAR) domain containing protein, SNX9 is known to deform the plasma membrane to induce membrane invagination (14-17).

SNX18 (sorting nexin 18), a sorting nexin family protein that is closely related to SNX9, has the same domain structure with SNX9 and expresses similarly to SNX9. Recent study, however, found that SNX9 and SNX18 localize differently in cells and appear to function in different trafficking pathways (18). Therefore, the exact function of SNX18 in related to SNX9 in CME should be clarified to find out whether it has redundant role or distinct role with SNX9.

During CME, SNX9 and SNX18 interact with various endocytic proteins as well as phosphoinositides, which are known to be affected to cause synaptic dysfunctions during early stages of Alzheimer's diseases (AD) (14, 19). In AD, the soluble Aβ oligomers are accumulated in brains, which is highly correlated with memory related synaptic dysfunctions (20-21). Recent studies discover that the soluble Aβ oligomers significantly interfere with cognitive function, impair synaptic plasticity and decrease the level of synaptic proteins such as postsynaptic density-95 (PSD-95) and dynamin-1 in the hippocampus (22-26). These alterations are caused by activation of N-Methyl-D-aspartate (NMDA) receptor, and NMDA receptor-dependent pathways lead to synaptic dysfunction such as a neuronal loss and long-term potentiation (LTP) failure (27-29). In addition, Aβ oligomers are known to decrease the level of PIP_2 that controls signal transduction, actin dynamics, exo-endocytosis and the permeability of ion channels (30). Since the imbalance of PIP_2 level is known

to cause the defects in CME process (31), how and by what mechanism(s) Aβ oligomers affect CME process in the neurons should provide the better understanding as to the cellular mechanisms of synaptic dysfunction during early AD.

By answering these questions, I expect to provide the detailed descriptions about the interaction between SNX18 and other endocytic proteins/phospholipids during CME process and how any alterations in CME process in neurons cause synaptic dysfunctions which are well correlated with the early measurable memory and cognitive deficits observed in AD.

<CHAPTER 1>

SNX18 shares a redundant role with SNX9 and modulates endocytic trafficking at the plasma membrane

INTRODUCTION

Endocytic pathways take membrane receptors and extracellular components into the cell, leading to activation of intracellular signaling pathways. Although several distinct endocytic pathways are known, clathrin-mediated endocytosis is the best characterized. Clathrin-mediated endocytosis begins by gathering membrane proteins and lipids through interactions with cytosolic adaptors and accessory factors, which bind to clathrin and initiate polymerization of triskeletal clathrin molecules into a spherical basket of clathrin-coated pits (CCPs) (2-3). Subsequently, the accessory proteins, such as amphiphysin, endophilin and sorting nexin 9 (SNX9), are concentrated at the membrane, inducing membrane curvature and the formation of intermediate tubular membrane structures (4-6, 10, 14). Finally, dynamin cuts off the tubular necks and releases the clathrin-coated vesicle into the cytoplasm (7-9). Proteins with membrane tubulating activity commonly have a Bin-Amphiphysin-Rvs (BAR) domain and a Src homology 3 (SH3) domain (15-16, 32-33). Recent crystal structures of the BAR domains of amphiphysin and endophilin revealed that the BAR domain forms a banana-shaped dimer that deforms the membrane to form tubular structures in vitro and in vivo (5, 34-35). The SH3 domain is involved in interactions with endocytic proteins and actin regulatory proteins such as dynamin and synaptojanin (13, 17, 36-37).

Dynamin plays a crucial role in clathrin-mediated endocytosis (38). Its N-terminal domain is responsible for GTP hydrolysis and its C-terminal proline-

rich domain (PRD) links it to SH3-domain-containing proteins such as amphiphysin, endophilin and SNX9. The central pleckstrin homology (PH) domain controls the binding of dynamin to membrane phospholipids (39). A coiled-coil domain (also called the GTPase effector domain or GED) that follows the PHD might play an important role in dynamin self-assembly and regulation of GTPase activity. There are three known isoforms of dynamin in mammals. Dynamin-1 is dominantly expressed in neuronal cells and contributes to synaptic-vesicle recycling (40-41). Dynamin-2 is expressed ubiquitously and its function is similar to that of dynamin-1 (42-43). Dynamin-3 is expressed in testis, but its function is still not well understood (44).

Recently, evidence has shown that SNX9 plays a key role in clathrin-mediated endocytosis (14, 17, 45-47). SNX9 forms a complex with dynamin in the cytosol and regulates the recruitment of dynamin to the membrane (48). Furthermore, SNX9 enhances dynamin assembly and increases its GTPase activity (17). Other endocytic molecules and actin regulatory proteins, adaptor protein complex 2 (AP-2), the Arp2/3 complex and clathrin also bind to the low-complexity (LC) region of SNX9 in a cooperative manner (14, 45-46). The SNX family contains two proteins that are closely related to SNX9: SNX18 and SNX33. All three have the same domain structure. An SH3 domain at the N terminus is followed by an LC domain of variable length, with a Phox homology (PX)-BAR region at the C terminus. It has been suggested that SNX18 and SNX33 branched off from SNX9, and were then duplicated (18). Because SNX9 has a crucial role in clathrin-mediated

endocytosis, it is of interest to also investigate the expression and function of SNX18 and SNX33.

A recent paper showed that SNX9, SNX18 and SNX33 localize differently in cells and appear to function in different trafficking pathways (18). Whereas SNX9 localizes to plasma membrane endocytic sites, SNX18 is found on peripheral endosomal structures. The LC domain of SNX18 contains a binding motif for adaptor protein complex 1 (AP-1) and it colocalizes with PACS1, but not with clathrin. SNX18 functions in an endosomal trafficking pathway that does not rely on clathrin, but is dependent on AP-1 and the retrograde trafficking protein PACS1 (18).

Here, however, it was shown that SNX18 and SNX9 are functionally redundant, and that SNX18 has a similar role to SNX9 in clathrin-mediated endocytosis, rather than a distinct role in endosomal trafficking. SNX18 and SNX9 are expressed together in most cell lines, but to a different extent. For example, SNX9 is dominantly expressed in HeLa cells and COS-7 cells, whereas SNX18 is dominantly expressed in the C6 glioma cell line. SNX18 interacts with dynamin, neuronal Wiskott-Aldrich syndrome protein (N-WASP) and synaptojanin – well-known binding partners of SNX9. SNX18 stimulates the basal GTPase activity of dynamin and regulates its recruitment to the plasma membrane. SNX18 can form homodimers and heterodimers with SNX9, and they colocalize in tubular membrane structures when overexpressed. Unlike the previous report (18), it could not be detected any colocalization of SNX18 with AP-1 or a cation-independent mannose-6-phosphate receptor (CI-MPR). SNX18 colocalizes with neither 2xPH

(FAPP1), a *trans*-Golgi marker, nor 2xFYVE (Hrs), an endosome marker. Instead, it colocalizes with clathrin and dynamin at the plasma membrane. In addition, SNX18 successfully replaced SNX9, such that defects in transferrin internalization caused by the depletion of SNX9 in HeLa cells are recovered by compensatory expression of SNX18 and vice versa. Depletion of SNX18 in C6 glioma cells caused endocytic defects. Using total internal reflection fluorescence (TIRF) microscopy in living cells, it was detected a transient burst of SNX18 recruitment to CCPs that coincides spatially and temporally with a burst of dynamin fluorescence and with a burst of SNX9; this occurs concomitantly with the disappearance of clathrin fluorescence. Taken together, these results are suggested that SNX18 functions in multiple endocytic trafficking pathways at the plasma membrane, rather than in a distinct endosomal trafficking pathway, and that SNX18 and SNX9 are functionally redundant.

MATERIAL AND METHODS

DNA constructs

SNX18, SNX9 and N-WASP were amplified by PCR and the PCR products were subcloned into pEGFP (Clontech, Mountain View, CA, USA), HA, Flag (modified from pEGFP-c1 vector), pTagRFP (Evrogen, Moscow, Russia) and pGEX-4T1 (Amersham Biosciences, Piscataway, NJ) vectors. The following constructs were PCR amplified and subcloned into expression vectors: SNX18-SH3 domain (residues 1-70), SNX18-ΔSH3 domain (residues 71-614), SNX18-BAR domain (residues 366-614), SNX18-ΔBAR domain (residues 1-385), SNX18-SH3LC domain (residues 1-265), SNX9-SH3 (residues 1-67), SNX9-ΔSH3 (residues 68-595) and SNX9-ΔBAR (residues 1-356). mRFP-Dyn2 (baa) and LCa-mRFP were kindly provided by Pietro De Camilli (Yale University, New Haven, CT, USA). RFP-2xPH (FAPP1) and GFP-2xFYVE (Hrs) were provided by Valker Haucke (Freie Universität Berlin, Berlin, Germany). All DNA constructs were verified by DNA sequencing.

Antibodies and reagents

The following antibodies were used. Anti-SNX18 rabbit polyclonal antibody was made by immunizing with GST-SH3-SNX18. Anti-SNX9 (Santa Cruz Biotechnology, Santa Cruz, CA), anti-dynamin-1 (ABR, Golden, CO, USA), anti-Hudy2 (Upstate Biotechnology, Lake Placid, NY, USA), anti-synaptojanin (Synaptic Systems, Göttingen, Germany), anti-GFP (Abcam, Cambridge, UK), anti-FLAG and anti-AP-1 (Sigma, St Louis, MO, USA),

anti-N-WASP (Chemicon, Temecula, CA, USA), anti-HA (Covance, Princeton, NJ, USA), anti-CI-MPR (AbD Serotech, Oxford, UK) and anti-clathrin (Thermo Scientific, Rockford, IL, USA) were used. Secondary antibodies were obtained from Jackson ImmunoResearch (West Grove, PA, USA). AlexaFluor594-dextran, Texas Red-transferrin and AlexaFluor488-transferrin were from Molecular Probes (Eugene, OR, USA). PDGF-BB was from Calbiochem (San Diego, CA, USA) and all other reagents were from Sigma.

Cell culture, transfection and immunocytochemistry

All cell lines were cultured at 37°C and 5% CO_2 in DMEM (Invitrogen, San Diego, CA, USA) supplemented with 10% FBS (Hyclone, Logan, UT, USA). Transfection was carried out using Lipofectamine 2000 (Invitrogen) and cells were observed after 16-24 hr. For immunocytochemistry, cells were fixed in 4% formaldehyde, 4% sucrose, PBS for 15 min, permeabilized for 5 min in 0.25% Triton X-100, PBS and blocked for 30 min in 10% BSA, PBS at 37°C. The cells were incubated with primary antibodies, 3% BSA, PBS for 2 hr at 37°C or overnight at 4°C, washed in PBS, and incubated with secondary antibodies, 3% BSA, PBS for 45 min at 37°C.

Microscopy

Confocal images were acquired on an Olympus FV-1000 confocal microscope with a 60X, 1.35 NA oil lens driven by FluoView 1000. Cells were excited

with 488 nm (from an argon laser) and 559 nm light (from a diode laser). For TIRF microscopy, cells were imaged using an Olympus IX-71 microscope fitted with a 60X 1.45 NA TIRF lens and controlled by Cell^{M} software (Olympus). Laser lines (488 and 561 nm diode lasers) were coupled to the TIRF microscopy condenser through two independent optical fibers. The calculated evanescent depth was <150 nm. Cells were typically imaged in two channels by sequential excitation with 0.1 to 0.2 second exposures and detected with a back-illuminated Andor iXon 897 EMCCD camera (512X512, 16 bit; Andor Technologies, Belfast, Northern Ireland). The Image J program (National Institutes of Health) was used for analysis.

Protein knock down and transferrin uptake assay

shRNA for SNX9 (human) was described previously (14). SNX18 shRNA (rat) was designed from nucleotides 1239-1260. Complementary oligonucleotides were synthesized separately, with the addition of an *Apa*I site at the 5' end and an *Eco*RI site at the 3' end. The target sequence of shRNA was 5'-GAGGTGGAGAGCAAGATAGAT-3'. The annealed cDNA fragment was cloned into the *Apa*I-*Eco*RI sites of the pU6-mRFP vector (insert DsRed sequences to pSilencer.U.1.0 vector, Ambion). After transfection, the cells were incubated for 48 hr for immunoblotting and transferrin-uptake assay. The transferrin-uptake assay was carried out as previously described (31). Briefly, 3 days after transfection, cells were starved for 6-8 hr in serum-free DMEM with 0.1% BSA and incubated in serum-free DMEM-HEPES containing 20 μg/ml Alexa488-transferrin (Invitrogen) for 10

min at 37°C. Cells were washed in acid-stripping solution (150 mM NaCl, 2 mM $CaCl_2$ and 25 mM CH_3COONa, pH 4.5) and fixed in 4% paraformaldehyde. Fluorescent images were taken under a confocal microscope and analyzed using MetaMorph software (Molecular Devices, Downingtown, PA, USA). The outline of the cell shape was drawn in the DIC images and average fluorescence intensity per cell was measured. Then, the fluorescent intensity of transfected cells was normalized against that of non-transfected cells.

GST pull-down assays

The GST-SNX18-SH3, GST-SNX9-SH3 and GST-virgin vector plasmids were transformed into *Escherichia coli* BL-21. The transformants were cultured in 2XYT medium supplemented with ampicillin. After overnight induction with 0.5 mM isopropyl 1-thio-β-D-galactopyranoside at 25°C, the cultures were sonicated in lysis buffer [1% Triton X-100, 0.5% sodium deoxycholate, 20 mM Tris, pH 8.0, 150 mM NaCl, 1 mM $MgCl_2$, 1 mM EGTA, 0.1 mM phenylmethylsulphonyl fluoride (PMSF)] and centrifuged at 15,000 ***g*** for 15 min. The supernatants were incubated with glutathione-agarose-4B beads (Amersham Biosciences) at 4°C for 1 hr. After washing three times with lysis buffer, the beads were incubated at 4°C for 2 hr with brain lysates in lysis buffer. The beads were then washed extensively with lysis buffer and analyzed by SDS-PAGE and immunoblotting. To assess in vitro binding, the SNX9-His plasmid was transformed into *E. coli* BL-21. The transformants were cultured in 2XYT medium supplemented with ampicillin.

After overnight induction with 0.5 mM isopropyl 1-thio- β-D-galactopyranoside at 25°C, the cultures were sonicated in NTA-lysis buffer (1% Triton X-100, 50 mM NaH_2PO_4, pH 8.0, 300 mM NaCl, 10 mM imidazole, 1 mM PMSF) and centrifuged at 15,000 ***g*** for 15 min. The supernatants were incubated with Ni-NTA chelating agarose CL-6B (Peptron Inc., Daejeon, Korea) at 4°C for 1 hr. After washing three times with NTA-washing buffer (0.1% Triton X-100, 50 mM NaH_2PO_4, pH 8.0, 300 mM NaCl, 20 mM imidazole, 1 mM PMSF), the beads were incubated at 4°C for 2 hr with NTA elution buffer (0.1% Triton X-100, 50 mM NaH_2PO_4, pH 8.0, 300 mM NaCl, 300 mM imidazole). The eluted product was quantified by SDS-PAGE and subsequently used for in vitro binding experiments. SNX9-His was incubated at 4°C for 2 hr with purified GST or GST fusion proteins bound to glutathione beads in lysis buffer. The beads were then washed extensively and analyzed by SDS-PAGE and immunoblotting.

In-gel digestion and peptide sample preparation

The SDS-polyacrylamide gels were silver stained and protein bands were excised. The resulting samples were washed three times with a 1:1 (v/v) solution of acetonitrile and deionized water for 10 min, dehydrated with 100% acetonitrile, washed with a 1:1 (v/v) solution of 100% acetonitrile and 100 mM ammonium bicarbonate, and dried using a SpeedVac. They were then reduced with 10 mM tris(2-carboxyethyl)phosphine hydrochloride in 0.1 M ammonium bicarbonate at 56°C for 45 min and alkylated with 55 mM iodoacetamide in 0.1 M ammonium bicarbonate at room temperature for 30

min. The above washing step was repeated on the alkylated samples, which were dried, soaked in sequencing-grade trypsin solution (500 ng) on ice for 45 min, and immersed in 100 ml of 50 mM ammonium bicarbonate pH 8.0 at 37°C for 14-18 hr. The resulting peptides were extracted sequentially by agitation for 20 min with 45% acetonitrile in 20 mM ammonium bicarbonate, 45% acetonitrile in 0.5% trifluoroacetic acid, and 75% acetonitrile in 0.25% trifluoroacetic acid. The extracts containing tryptic peptides were pooled and evaporated under vacuum.

Micro-LC-MS/MS analysis and protein database search

In-gel digested proteins were loaded onto fused silica capillary columns (100 μm inner diameter, 360 μm outer diameter) containing 8 cm of 5 μm particle size Aqua C18 reverse-phase column material. The columns were placed in line with an Agilent HP 1100 quaternary LC pump and a splitter system was used to achieve a flow rate of 250 nl /min. Buffer A (5% acetonitrile and 0.1% formic acid) and buffer B (80% acetonitrile and 0.1% formic acid) were used to make a 90 min gradient. The gradient profile started with 5 minof 100% buffer A, followed by a 60 min gradient from 0% to 55% buffer B, a 25 min gradient from 55% to 100% buffer B, and a 5 min gradient of 100% buffer B. Eluted peptides were directly electrosprayed into an LTQ linear ion trap mass spectrometer (ThermoFinnigan, Palo Alto, CA, USA) by applying 2.3 kV of DC voltage. Data-dependent scans consisting of one full MS scan (400-1400 m/z) and five data-dependent MS/MS scans were used to generate MS/MS spectra of the eluted peptides. Normalized collision energy of 35% was used

throughout data acquisition. MS/MS spectra were searched against an NCBI rat protein sequence database using Bioworks version 3.1 and Sequest Cluster System (14 nodes). DTASelect was used to filter the search results and the following Xcorr values were applied to the different charge states of peptides: 1.8 for singly charged peptides, 2.2 for doubly charged peptides and 3.2 for triply charged peptides. Fragment ions in each MS/MS spectrum were manually assigned to confirm the database search results.

Coimmunoprecipitation and immunoblotting

To detect SNX18 and SNX9 binding to N-WASP in vivo, 293T cells were transfected with GFP, GFP-SNX18, GFP-SNX18-ΔSH3, GFP-SNX9 and GFP-SNX9-ΔSH3 together with HA-N-WASP using Liopofectamine 2000 (Invitrogen). The cells were washed twice with cold PBS and extracted at 4°C for 1 hr in a modified RIPA buffer (50 mM Tris-HCl pH 7.5, 5 mM EDTA, 150 mM NaCl, 1% Nonidet P-40, 1 mM sodium orthovanadate, 1 mM PMSF, 10 mM leupeptin, 1.5 mM pepstatin, and 1 mM aprotinin). They were then clarified by centrifugation at 15,000 ***g*** for 15 min and protein concentrations were determined with a Bradford protein assay reagent kit (Bio-Rad). Samples containing 1 mg of total protein were immunoprecipitated for 4 hr with anti-GFP antibody, followed by an additional 2 hr of incubation at 4°C with protein A-Sepharose beads (Amersham Biosciences). The immunoprecipitates were extensively washed with lysis buffer, subjected to SDS-PAGE and transferred to a polyvinylidine difluoride membrane (Bio-Rad). The membrane was blocked with 5% skim milk TBST (10 mM Tris-

HCl, 100 mM NaCl and 0.1% Tween-10, pH 7.5) for 1 hr, washed and probed with primary antibody for 1 hr at room temperature. After extensive washing in TBST, the membrane was incubated with horseradish peroxidase (HRP)-conjugated secondary antibody (Jackson ImmunoResearch Laboratories). Proteins were visualized with enhanced chemiluminescence reagent (Amersham Biosciences). To examine homodimerization and heterodimerization of SNX18 and SNX9, 293T cells were transfected with various GFP-tagged SNX18 and SNX9 wild types and their mutants, together with FLAG-SNX18 using Lipofectamine 2000.

In situ hybridization

In situ hybridization on mouse E16, E18, P3, P7, P18 and adult brain sections was carried out with digoxigenin-labeled SNX18 RNA antisense probes and detected with anti-digoxigenin antibodies coupled to alkaline phosphatase (Roche Applied Biosystems, Pleasanton, CA, USA) and nitro blue tetrazolium-5-bromo-4-chloro-3-indolyl phosphate color substrate.

Native dynamin I purification and GTPase assay

Dynamin I was purified from mouse brain as described previously (49). Briefly, amphiphysin-I-SH3-GST was immobilized on agarose beads and incubated with brain lysate for 2 hr. Bound dynamin I was eluted from amphiphysin-I-SH3-GST using a high salt elution buffer (1.2 M NaCl, 20 mM PIPES, 1 mM DTT, pH 6.5). The eluted dynamin I protein was placed in a

diluting buffer (30 mM Tris/HCl, 100 mM NaCl pH 7.4) and quantified by SDS-PAGE. Dynamin I GTPase activity was measured using the GTPase Enzyme Linked Inorganic Phosphate Assay (ELIPA; Cytoskeleton Inc., Denver, CO, USA). Briefly, 1 μM dynamin I was mixed with 1 μM of SNX9 or SNX18. These protein mixtures were added to prepared ELIPA mixture with 1 mM GTP. A monochromatic spectrophotometer PowerWave XS (BioTek instruments, Winooski, VT, USA) was used to measure the amount of phosphate released by GTP hydrolysis and checked by absorbance at 360 nm using a kinetics assay with a 1 min interval.

Dextran uptake

NIH cells were grown on coverslips at 37°C for 1 day and then transfected with SNX18-shRNA using Lipofectamine 2000 (Invitrogen). Two days after transfection, cells were incubated in the presence of 10 kDa AlexaFluor594-dextran (Invitrogen) with PDGF-BB (Calbiochem), fixed with 4% paraformaldehyde and mounted on coverslips. Fluorescence images were acquired on an Olympus IX-71 inverted microscope.

RESULTS

Expression of SNX18 in various cell lines and during development

To assess the cellular distribution of SNX18, an antibody was raised against recombinant SNX18 (Figure 1-1, 1-2). Immunoblotting analysis was carried out in different cell lines from different species to compare its distribution with that of SNX9. Most cell lines expressed both proteins, but to a different extent. SNX9 was dominantly expressed in HeLa, TM4, L929 and COS-7 cells, whereas SNX18 was more strongly expressed than SNX9 in C6, Ha-CAT, HL-1 and NIH-3T3 cells (Figure 1-3B).

To investigate the tissue distribution of SNX18 during development, the expression of *SNX18* mRNA was examined by in situ hybridization with parasagittal sections of whole embryos (E16 and E18) or coronal sections of postnatal mouse brains (P3, P7 and adult) (Figure 1-3C). SNX18 is widely expressed in the developing embryos. On E16, *SNX18* mRNA signals were found throughout the CNS and various peripheral tissues, including liver, lung, heart, thymus and intestine. On E18, the expression of SNX18 was decreased compared with that on E16. On P3, SNX18 expression was found in the outer layer of the cerebral cortex, hippocampal formation, external germinal layer of the cerebellum and internal capsule. Similar expression patterns were maintained on P7-P18. At these stages, *SNX18* mRNA was found in the external germinal layer (P7) and granular layer (P18) of the cerebellum. In addition, the mRNA signal was also prominent in the external capsule. In the

adult mouse brain, substantial expression of *SNX18* mRNA was observed in the hippocampal formation and cerebellum. In addition, moderate level of signal was found in the glomerular layer of the olfactory bulb.

SNX18 interacts with dynamin, N-WASP and synaptojanin

Because SNX18 contains an SH3 domain and its SH3 domain is similar to that of SNX9, it could bind PRD-containing proteins. To identify proteins that interact with the SH3 domain of SNX18, it was carried out a series of GST pull-down assays and performed a micro-LC-MS/MS analysis (Figure 1-4A). Brain lysates were pulled down with GST-SNX18, GST-SH3-SNX18 and GST-ΔSH3-SNX18, and SDS-polyacrylamide gels were silver stained. After in-gel digestion, micro-LC-MS/MS and a protein database search identified dynamin, N-WASP and synaptojanin (Figure 1-4A). GST pull-down assays followed by immunoblotting with specific antibodies further confirmed that SNX18 interacts with dynamin, synaptojanin-1 and N-WASP (Figure 1-4B), as does SNX9 (47, 50).

SNX18 stimulates the basal GTPase activity of dynamin and its recruitment to the plasma membrane

SNX9 binds to dynamin and stimulates its basal GTPase activity (17). To determine whether the interaction of SNX18 and dynamin regulates aspects of dynamin activity, it has been measured the basal rate of GTP hydrolysis of

dynamin in the presence of GST-SNX18. Figure 1-5A shows that GST-SNX18 stimulated the basal GTPase activity of dynamin-1; this is fully comparable to the action of GST-SNX9.

To see whether SNX18 affects the localization of dynamin, C6 glioma cells (where SNX18 is dominantly expressed and SNX9 is almost absent; see Figure 1-3B) were co-transfected with dynamin-2–GFP and either SNX18 short hairpin RNA (shRNA) or mock vector. TIRF imaging was then performed. It was found that the membrane recruitment of dynamin-2 was significantly lower in SNX18 knock down cells compared with control cells (Figure 1-5B, C). This is consistent with the previous report regarding the role of SNX9 in dynamin localization (51).

SNX18 and SNX9 form a heterodimer, and are colocalized on membrane tubules when overexpressed

SNX18 contains a BAR domain, suggesting that it can dimerize and oligomerize. Indeed, SNX18 homodimerizes and heterodimerizes with SNX9 in vivo and in vitro, and does so by means of its BAR domain (Figure 1-6A, B). BAR-domain-containing proteins are known to trigger membrane deformation and invagination, known to be required for the formation of intermediate structures during clathrin-mediated endocytosis (15, 32, 34). When overexpressed, these proteins induce the formation of massive membrane tubules. It has been shown that SNX9 can induce membrane tubules, which requires its PX and BAR domains. SNX18 also contains PX

and BAR domains and, as recently shown, SNX18 can also tubulate the plasma membrane (Figure 1-6C, D). Live confocal microscopy showed that SNX18-GFP and SNX9-mRFP colocalized with each other on the tubules, rather than showing patch overlap, as has been found in a recent study (18). This is consistent with results of Figure 1-4 that they could form a heterodimer (Figure 1-6C, D).

SNX18 localizes at the cell surface, where it is partially colocalized with clathrin and dynamin

A previous study showed that endogenous SNX18 colocalizes with AP-1 and PACS1-positive endosomal structures, which are devoid of clathrin (18). According to immunostaining studies in here, however, showed that endogenous SNX18 colocalizes neither with AP-1, a late endosome marker (Figure 1-7A-D), nor with CI-MPR, a *trans*-Golgi marker (Figure 1-8). TIRF microscopy was used to visualize the proteins in the vicinity of the plasma membrane and clearly showed that endogenous SNX18 colocalizes not with AP-1 (Figure 1-7D), but rather partially with clathrin and dynamin at the cell surface (Figure 1-9A, B).

Consistent with their heterodimerization, endogenous SNX18 and SNX9 were colocalized at the cell surface as well (Figure 1-9C).

When exogenously expressed, SNX18 colocalized neither with RFP-2xPH (FAPP1), a PtdIns(4)*P* marker, nor with GFP-2xFYVE (Hrs), a PtdIns(3)*P* marker, suggesting that it is not located in the Golgi complex or in early

endosomes (Figure 1-10). This result is consistent with the previous report showing that SNX18 has a preference for PtdIns(4,5)P_2 lipids, which are enriched in the plasma membrane (18).

SNX18 can replace the function of SNX9 during clathrin mediated endocytosis

Considering the structural similarity of SNX18 and SNX9, and the fact that they share binding partners, SNX18 could have a role in clathrin-mediated endocytosis. In fact, knocking down endogenous expression of SNX18 using shRNAs inhibits transferrin uptake in C6 glioma cells, where SNX18 is dominantly expressed (Figure 1-11A, B and Figure 1-12). Next, it was wondered whether SNX18 could compensate for lack of SNX9 during clathrin mediated endocytosis and vice versa. In order to answer this question, it was overexpressed SNX18 or SNX9 in a SNX9 or SNX18 knock-down background, respectively. SNX9 or SNX18 knock-down resulted in defective transferrin uptake in HeLa cells or C6 glioma cells, where SNX9 or SNX18 is dominantly expressed, respectively. SNX9 successfully rescued the endocytic defects caused by SNX18 depletion in C6 glioma cells (Figure 1-11A, B) whereas the endocytic defects caused by SNX9 depletion in HeLa cells were rescued by cotransfection of SNX18 (Figure 1-11C, D). These results suggest that SNX18 plays a similar role to SNX9 during clathrin-mediated endocytosis.

Mutants of SNX9 and SNX18 with their SH3 domain deleted (ΔSH3-SNX9

in Figure 1-11A, B and ΔSH3-SNX18 in Figure 1-11C, D) only partially rescued the endocytic defects caused by either SNX18 or SNX9 depletion, suggesting that full-length SNX9 or SNX18 is required for complete rescue. This is conceivable considering that SNX18 and SNX9 are composed of four functional domains (SH3, LC, PX and BAR) that are known to bind a variety of proteins to regulate various steps of clathrin-mediated endocytosis (14, 46).

SNX18 is recruited to CCPs at a late stage

Next, it was investigated the spatiotemporal dynamics of SNX18 in live cells and its association with CCP turnover using TIRF microscopy. The partial colocalization of SNX18 with CCPs reflects the transient interaction of SNX18 with CCPs (Figure 1-9A). GFP-SNX18 and RFP-LCa (clathrin light chain) were transiently coexpressed in COS7 cells. Individual clathrin puncta appeared asynchronously, slowly increased in fluorescence intensity, plateaued and then rapidly disappeared. GFP-SNX18 colocalized as a transient burst with ~64% of the RFP-LCa spots, just before disappearance of the clathrin signal. Although there was some variability in the spatiotemporal relationship between SNX18 and clathrin, the peak of the SNX18 burst was observed to occur either just before or coincident with the disappearance of clathrin fluorescence from TIRF microscopy (Figure 1-13A-C). The kinetics of the SNX18 burst was reminiscent of the transient recruitment of dynamin. Therefore, it was examined the timing of SNX18 recruitment relative to dynamin-2. In most cases, 80% of the transient bursts of SNX18 colocalized with a burst of dynamin and the kinetics of changes in fluorescence intensity

were indistinguishable (Figure 1-13D, E). These results suggest that SNX18 and dynamin are transiently recruited to endocytic CCPs at a late stage of clathrin coated vesicle formation. Consistent with this data suggesting that SNX9 and SNX18 dimerize, when cotransfected, the kinetics of GFP-SNX18 fluorescence and RFP-SNX9 fluorescence were indistinguishable; ~76% of the transient burst of SNX18 colocalized with a burst of SNX9 (Figure 1-13F, G).

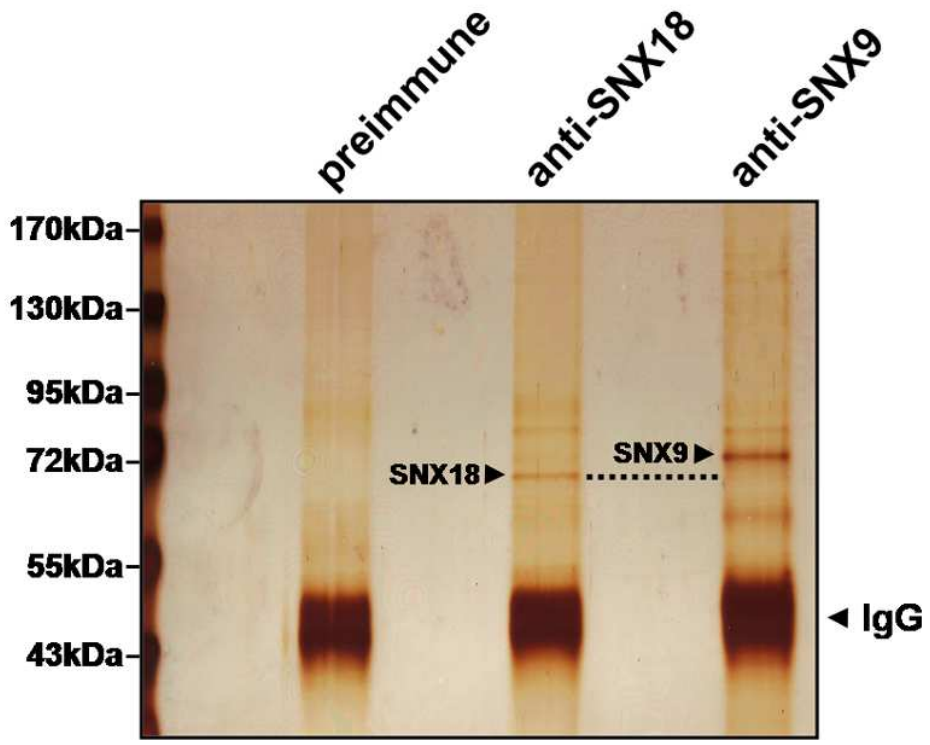

Figure 1-1. Anti-SNX18 and anti-SNX9 antibodies have no cross reactivity

HEK293T cell cytosol was immunoprecipitated with a preimmune serum, anti-SNX18 or anti-SNX9 antibodies, analyzed with SDS-PAGE and silver stained. Each antibody specifically identified each protein, not both, indicating no cross reactivity between antibodies. The dotted line indicates the size of SNX18 in gel.

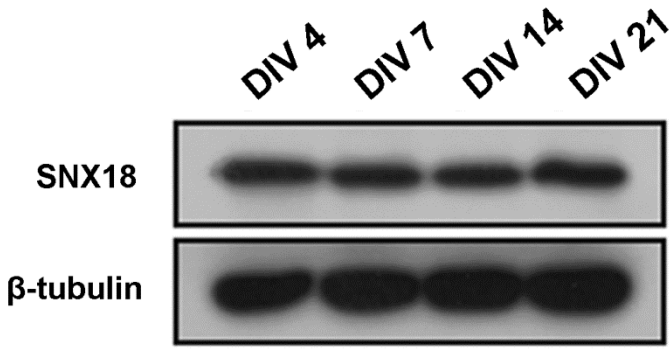

Figure 1-2. Expression patterns of SNX18 in culture rat hippocampal neurons.

Hippocampal neurons at 3, 7, 14 and 21 days in vitro in culture were lysed and immunoblotted with specific SNX18 antibody to show the expression of SNX18 at different developmental stages. β-tubulin was used as a reference.

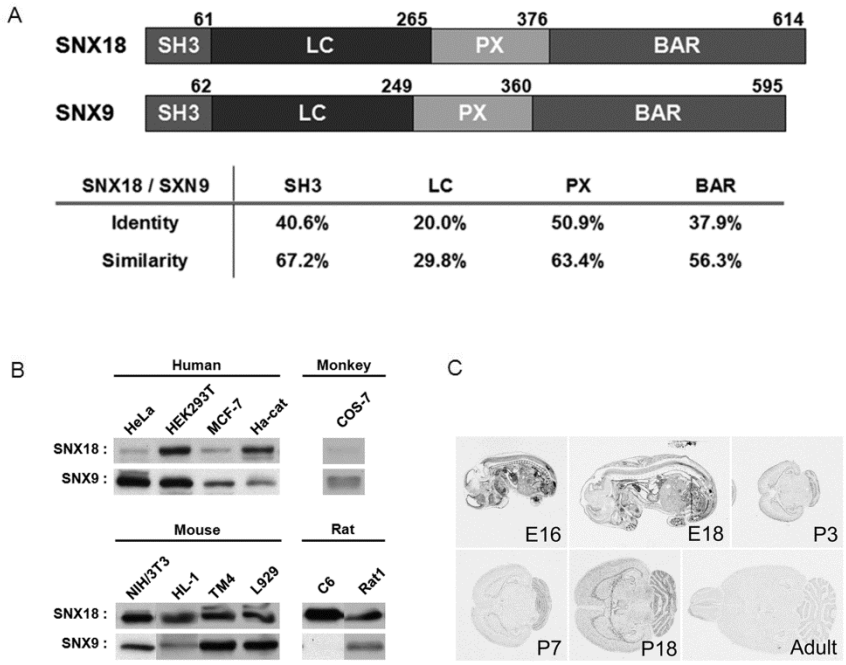

Figure 1-3. Expression patterns of SNX18 in various cell lines and during development.

(**A**) Schematic diagrams of SNX18 and SNX9 and their domain structures. Individual domain sequences were aligned with ClustalW software. (**B**) Immunoblotting analysis of different cell lines from different species using anti-SNX18 and anti-SNX9 antibodies. The same amount of protein was loaded in each lane. (**C**) In situ hybridization with parasagittal sections of whole embryos (E16 and E18) or coronal sections of postnatal mouse brains (P3, P7 and adult). Scale bar: 5.0 μm

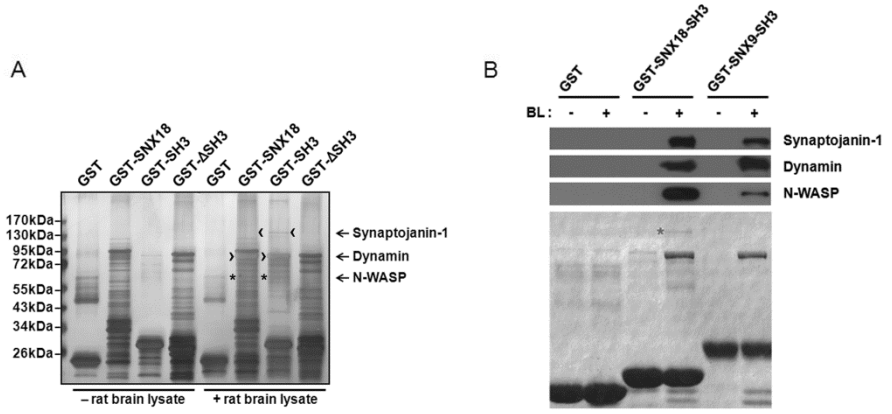

Figure 1-4. SNX18 interacts with dynamin, N-WASP and synaptojanin.

(**A**) Rat brain lysates were incubated with GST, GST-SNX18, GST-SNX18-SH3 and GST-SNX18-ΔSH3. SDS-polyacrylamide gels were stained with silver. Specific bands were excised from the stained gel, and analyzed by micro-LCMS/MS and by a protein database search, identifying synaptojanin (<), dynamin (>) and N-WASP (*). (**B**) GST fusion proteins of SNX18-SH3 and SNX9-SH3, and GST alone were incubated with rat brain lysates (BL) and SDS-polyacrylamide gels were stained with Coomassie Brilliant Blue. The proteins were transferred to a polyvinylidine difluoride membrane and immunoblotted with anti-synaptojanin antibody, anti-dynamin-1 antibody or anti-N-WASP antibody. The asterisk indicates the band including synaptojanin-1.

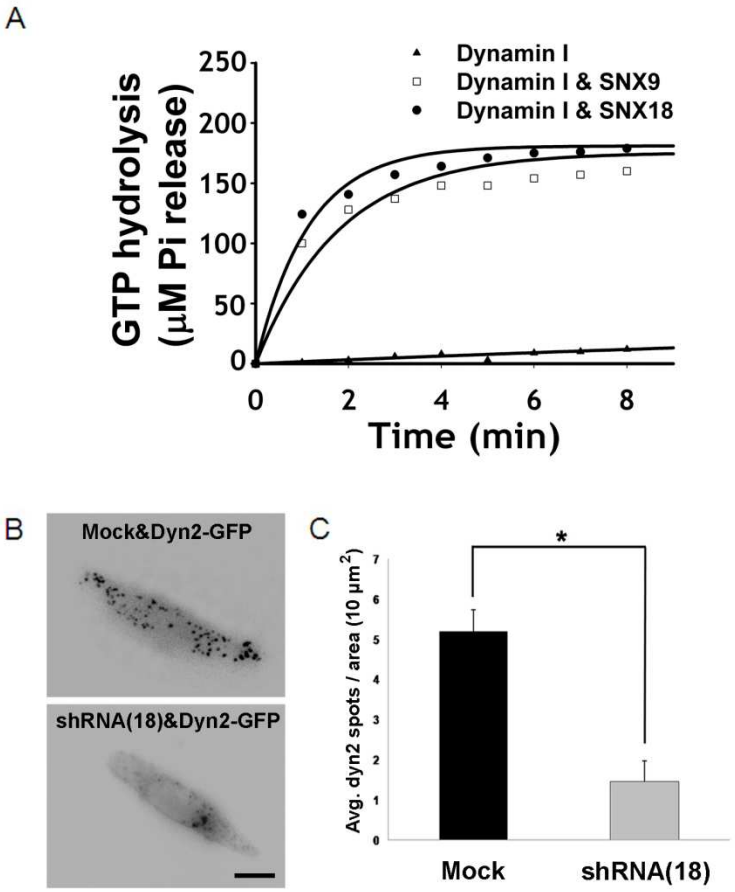

Figure 1-5. SNX18 stimulates the basal GTPase activity of dynamin and its recruitment to the plasma membrane.

(**A)** Basal dynamin-1 GTPase activity was measured using the GTPase ELIPA assay. 1 μm dynamin I was mixed with 1 μm GST-SNX18 or GST-SNX9, and added to prepared ELIPA mixture with 1 mM GTP. The amount of inorganic phosphate released by dynamin-1 only or in the presence of GST-SNX18 or

GST-SNX9 was measured at 360 nm with 1 min intervals and plotted as a function of time. (**B**) TIRF microscopy images of C6 glioma cells transfected with dynamin-2-GFP and mock, or SNX18 shRNA. Three days after transfection, cells were imaged using TIRF microscopy. Scale bar: 10 μm. (**C**) Bar graph indicating that SNX18 depletion in C6 cells blocks the recruitment of dynamin-2 to the plasma membrane. *Statistically significant at $P<0.05$, Student's *t*-test.

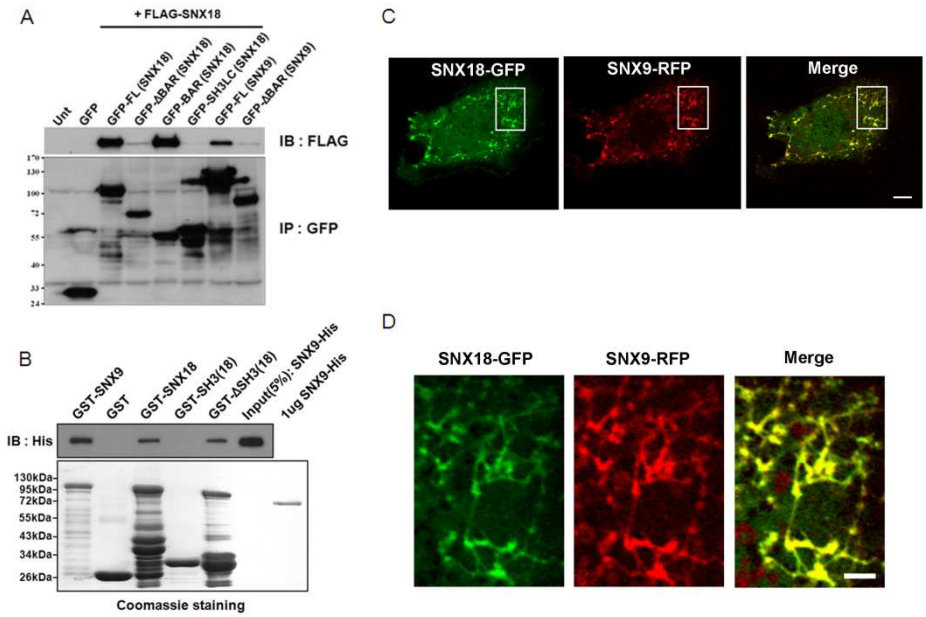

Figure 1-6. SNX18 and SNX9 form a heterodimer, and are colocalized on membrane tubules.

(**A**) HEK293T cells were co-transfected with GFP-FL(SNX18), ΔBAR(SNX18), BAR(SNX18), SH3LC(SNX18), FL(SNX9), ΔBAR(SNX9) or GFP alone, and FLAG-SNX18. 24 hr after transfection, the cells were lysed and immunoprecipitated (IP) with anti-GFP antibody, and immunoblotted (IB) with anti-FLAG antibody. Unt, untransfected; FL, full length. (**B**) In vitro binding assays were carried out with purified SNX9-His and GST-SNX9, GST-SNX18, ΔSH3 (SNX18), SH3 (SNX18) or GST alone, followed by immunoblotting with anti-His antibody. Input (5%):SNX9-His was used as a positive control. GST-SNX9, GST-SNX18 and GST-SNX18-

ΔSH3 but not GST-SNX18-SH3 bind to SNX9-His, confirming the direct interaction of SNX18 with SNX9. (**C**). COS-7 cells were transfected with SNX18-GFP and SNX9-mRFP, and time-lapse imaging was performed 14 hr after transfection. Scale bar: 10 μm (**D**). High-magnification views of the regions in (C) enclosed in rectangles. SNX18-GFP and SNX9-mRFP are colocalized on the membrane tubules. Scale bar: 2 μm.

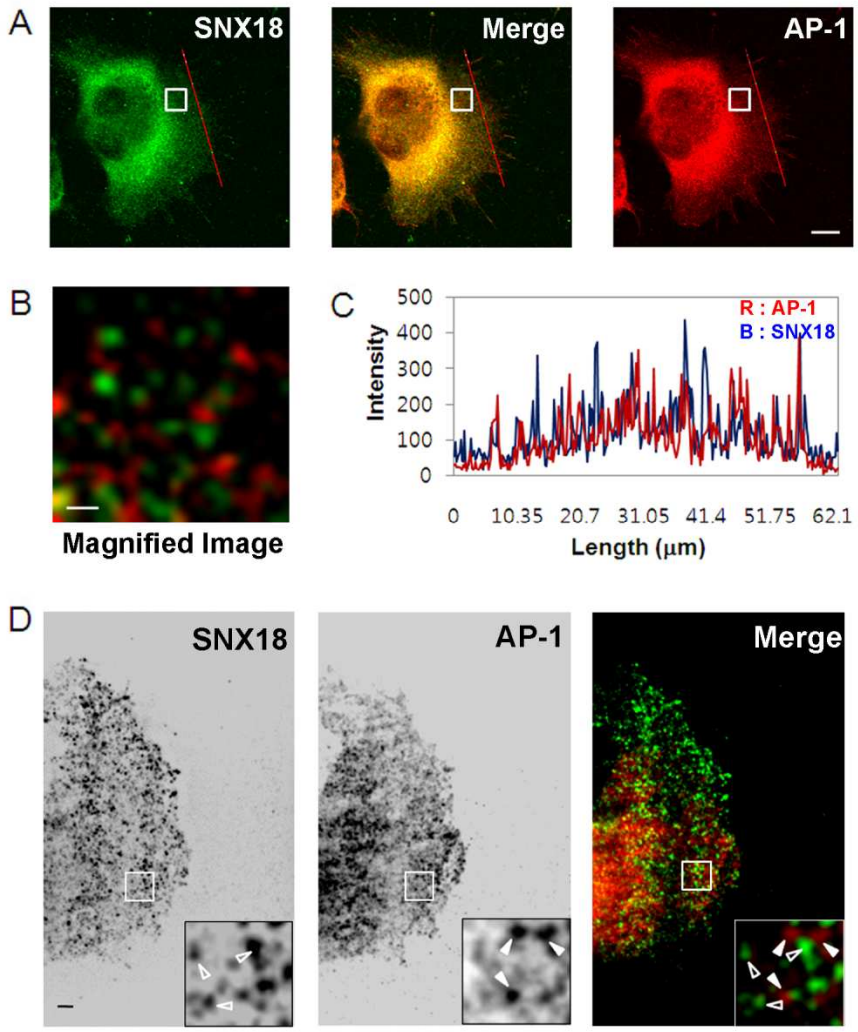

Figure 1-7. SNX18 does not colocalize with AP-1.

(**A-C**) Confocal micrographs of NIH3T3 cells co-stained for endogenous SNX18 and AP-1, and graph indicating the intensity profile of the red line in each image. AP-1 does not colocalize with SNX18. Scale bars: 10 μm (A), 1 μm (B). (**D**) TIRF microscopy images of NIH3T3 cells co-stained for endogenous SNX18 (left, green in merge) and AP-1 (middle, red in merge) show no colocalization (open arrowheads). Scale bar: 2 μm.

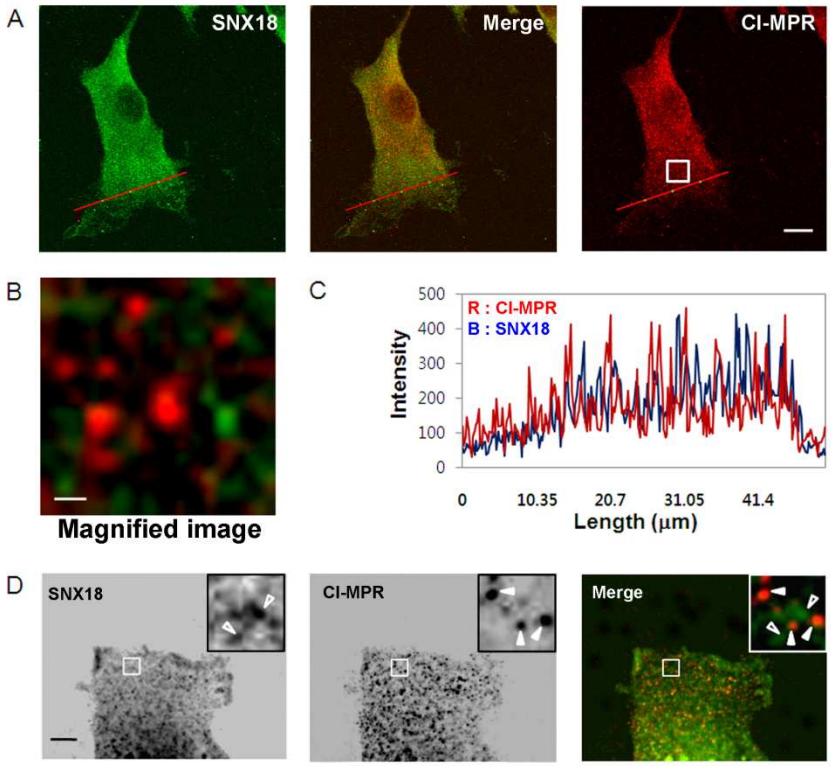

Figure 1-8. Endogenous SNX18 does not colocalize with CI-MPR.

(A-C**)** Confocal micrographs of NIH3T3 cells co-stained for endogenous SNX18 and CI-MPR, and graph indicating the intensity profile of the red line in each image. CI-MPR does not colocalize with SNX18. CI-MPR: cation-independent mannose-6-phosphate receptor. Scale bars: 10 μm (A), 1 μm (B). (**D**) TIRF microscopy images of NIH3T3 cells co-stained for endogenous SNX18 (left, green in merge) and CI-MPR (middle, red in merge) show no colocalization (open and filled arrowheads). Scale bar: 5 μm

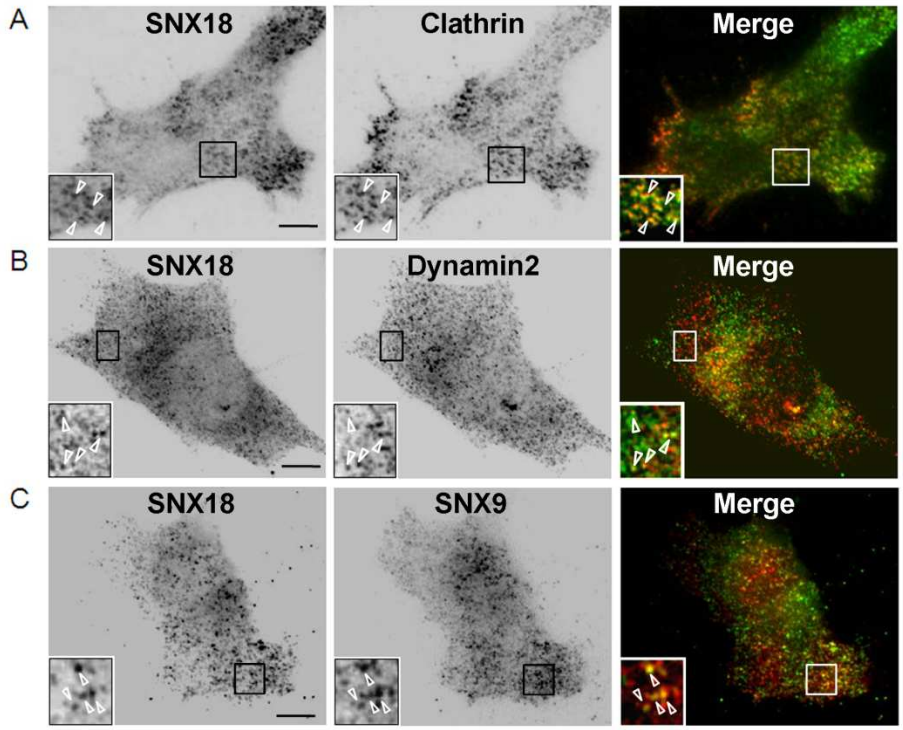

Figure 1-9. SNX18 localizes at the cell surface, where it is partially colocalized with clathrin, dynamin and SNX9.

TIRF microscopy images of NIH3T3 cells co-stained for endogenous SNX18 (left, green in merge) and clathrin **(A)**, dynamin-2 **(B)** or SNX9 **(C)** (middle, red in merge) show partial but considerable colocalization in the vicinity of the plasma membrane (open arrowheads). Scale bars: 10 μm.

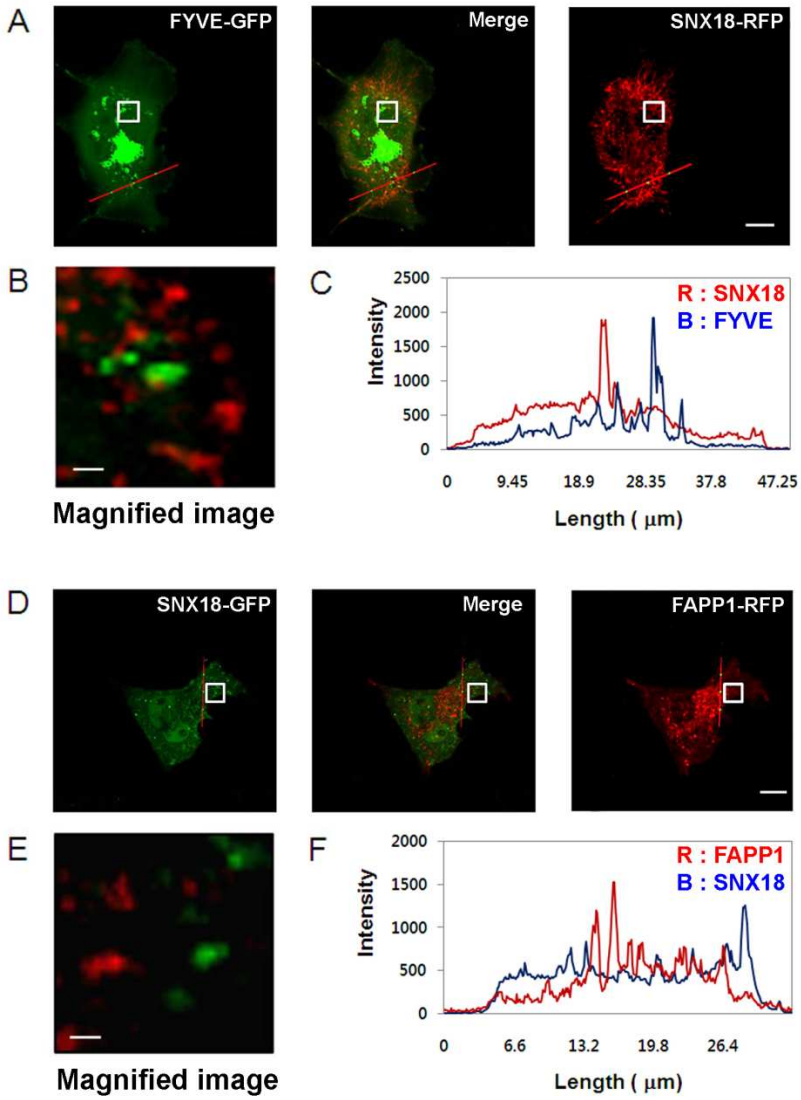

Figure 1-10. SNX18 does not localize with endosome marker, 2XFYVE.

Confocal micrographs of COS-7 cells transiently transfected with SNX18-RFP and FYVE-GFP (**A-C**), or SNX18-GFP and FAPP1-RFP (**D-F**). High-magnification views are of the regions enclosed in rectangles. The graphs indicate the intensity profile of the red line in each image. Scale bars: 10 μm (A,D), 1 μm (B,E).

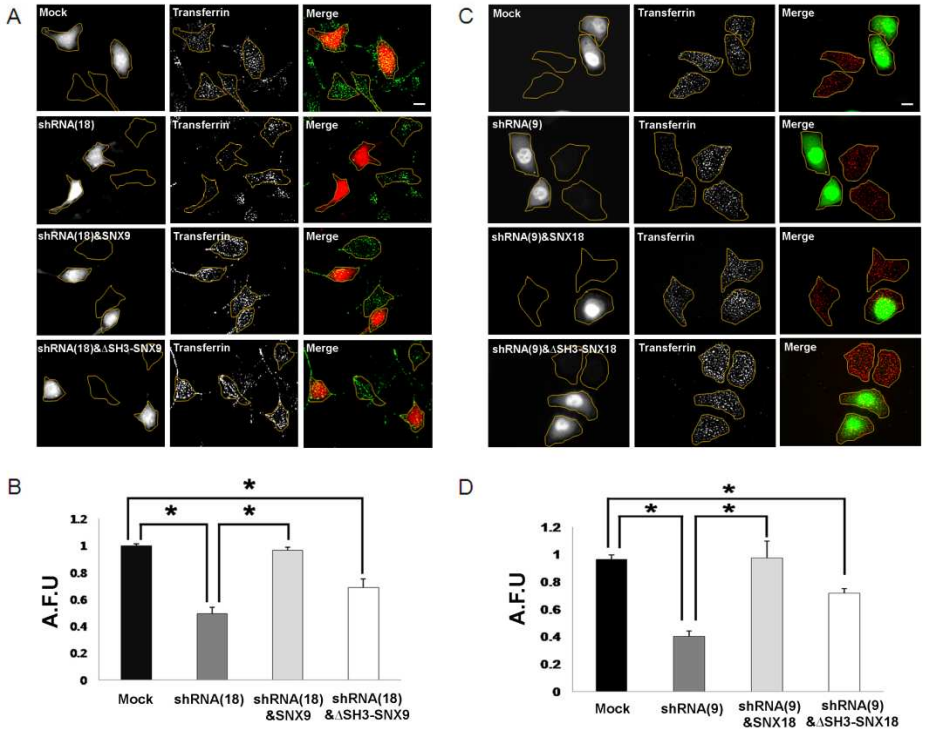

Figure 1-11. SNX18 is required for transferrin uptake and compensates for the lack of SNX9 during clathrin-mediated endocytosis and vice versa. (**A**, **B**) C6 glioma cells were transfected with mock, shRNA-SNX18, shRNA-SNX18 plus SNX9 and shRNA-SNX18 plus ΔSH3-SNX9. Three days after transfection, cells were incubated with AlexaFluor488-transferrin for 10 min. After fixing, the cells were examined using microscopy. Cells were outlined for better comparison. Knock down of endogenous SNX18 reduced transferrin uptake by 55%. SNX9 fully rescued endocytic defects caused by SNX18 depletion in C6 glioma cells, whereas the SH3-deleted mutant of SNX9 did so partially. (**C**, **D**) HeLa cells were transfected with mock, shRNA-SNX9,

shRNA-SNX9 plus SNX18 and shRNASNX9 plus ΔSH3-SNX18. Three days after transfection, cells were incubated with AlexaFluor488-transferrin for 10 min. Cells were outlined. Endocytic defects caused by SNX9 depletion in HeLa cells were fully rescued by SNX18 and partially rescued by SH3-deleted mutants of SNX18. These data demonstrate that SNX18 can replace the function of SNX9 in clathrin-mediated endocytosis and vice versa. Data are given as the mean ± s.e.; n=5. *Statistically significant at P<0.05, ANOVA and Tukey's HSD post hoc test for several different groups and Student's t-test for two different groups. Scale bar: 20 μm.

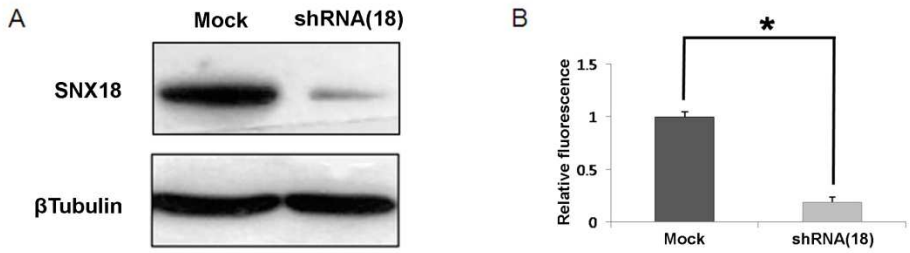

Figure 1-12. SNX18-shRNA is efficiently knockdown SNX18 expression.

(**A**) C6 glioma cells were transfected with mock or shRNA-SNX18, and lysates were immunoblotted with antibodies against SNX18 and β-tubulin. (**B**) Relative band intensities are displayed as histograms. *Statistically significant at $P<0.05$, Student's *t*-test.

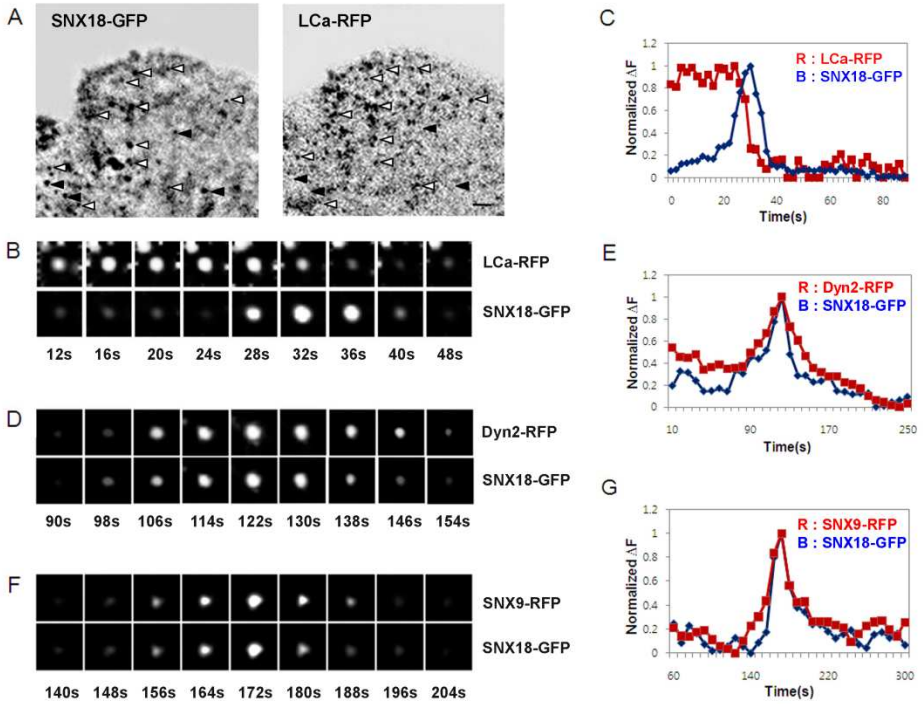

Figure 1-13. SNX18 is recruited to CCPs at a late stage in vesicle formation.

(**A**). TIRF microscopy images of a COS-7 cell co-transfected with SNX18-GFP and LCa-mRFP show colocalization (open arrowheads) or no colocalization (filled arrowheads). Scale bar: 2 μm. (**B**) Selected frames from a time-lapse sequence acquired every 2 seconds of a clathrin spot (top) and SNX18 spot (bottom). (**C**) Normalized fluorescence intensity changes as a function of time of a representative clathrin spot (red) and its corresponding 'burst' of SNX18 (blue). (**D-G**) Selected TIRF microscopy images from times series acquired every 2 seconds of dynamin-2 (D) or SNX9 (F), and SNX18. Normalized fluorescence graphs show spatial and temporal colocalization of SNX18 (blue) and dynamin-2 (E, red) or SNX9 (G, red).

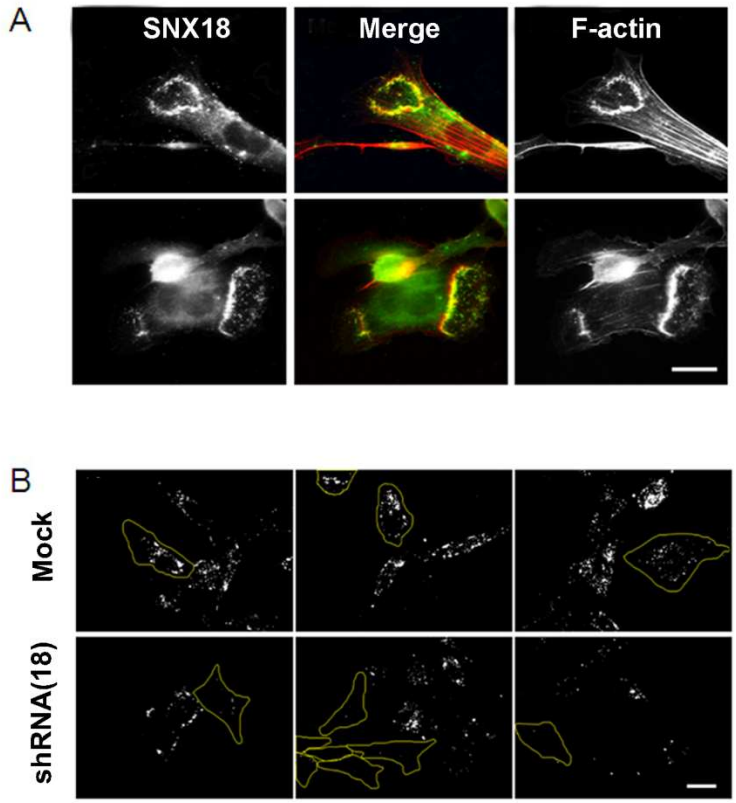

Figure 1-14. SNX18 is required for dorsal ruffle formation and fluid-phase endocytosis.

(**A**) SNX18 is enriched in dorsal ruffles. Fluorescence images of endogenous SNX18 (left, green in merge) and phalloidin staining of F-actin (right, red in merge) in PDGF-stimulated cells. Scale bar: 20 μm. (**B**) AlexaFluor594-dextran uptake via fluid-phase endocytosis is reduced in SNX18-depleted NIH3T3 cells. Fluorescence images of NIH3T3 cells treated with SNX18-shRNA or mock shRNA, and incubated for 8 min with 0.25 mg/ml AlexaFluor594-dextran. Scale bar: 20 μm.

DISCUSSIONS

SNX9 is now a well-understood protein that is required for clathrin-mediated endocytosis and clathrin-independent, actin-dependent fluid-phase endocytosis. SNX9 interacts with various proteins, such as dynamin, N-WASP, AP-2, Arp2/3 and phosphatidylinositol-4-phosphate-5-kinase-α, β (PIPkinase-α, β); these interactions are required for proper regulation of endocytosis (14). Vertebrate genomes express two proteins that are closely related to SNX9: SNX18 and SNX33 (18). These proteins constitute a separate subfamily of PX-BAR-containing SNX proteins. All three proteins contain similar domains: an N-terminal SH3 domain, LC and PX domains in the middle, and a C-terminal BAR domain (18). They have ~40-70% sequence identity in the different domains, with the lowest identity found in LC domain. It seems that the ancestor of SNX18 and SNX33 branched off from SNX9 and was duplicated. *Caenorhabditis elegans* has only one ortholog of SNX9, SNX18 and SNX33, termed *lst-4* (52). Overexpression of *lst-4* results in a phenotype very similar to a dynamin loss-of-function phenotype in *C. elegans*; this is consistent with previous results and current results regarding the interaction of SNX9 and SNX18 with dynamin during endocytosis (52).

Because SNX9 acts as a crucial regulator of vesicle trafficking, whether the three proteins have redundant roles or distinct roles in cells is of interest. Recent study showed that SNX33 binds dynamin and regulates amyloid precursor protein (APP) endocytosis in a dynamin-dependent manner. Also,

SNX9 has a similar effect on APP shedding and APP cell-surface level as SNX33, suggesting that they both function in endocytosis (52). Another study showed that overexpression of SNX33 impaired cellular prion protein (PrPc) endocytosis at the plasma membrane, supporting the crucial role of SNX33 in endocytosis at the plasma membrane (53). A recent study, however, showed that SNX9, SNX18 and SNX33 localize differently and might function in different trafficking pathways. It was shown that SNX18 binds dynamin, but participates in membrane remodeling at endosomes together with AP-1 and PACS1, rather than functioning in endocytosis at the plasma membrane as SNX9 does, casting doubt on their suggested redundant roles (18).

The current results support the conclusion that SNX18 plays a role in endocytic pathways at the plasma membrane. Although I cannot completely rule out the possibility that these proteins have distinct roles, I believe that SNX18 is a redundant protein in the same pathways as SNX9, for the following reasons. First, most of the cell lines tested express SNX9 and SNX18, but to a different extent. In particular, SNX9 is highly expressed in HeLa and COS-7 cells, with quite low expression of SNX18, whereas the opposite is true in C6 glioma cells. Second, SNX18 interacts with dynamin, N-WASP and synaptojanin, well-known binding partners of SNX9. Third, knock down of SNX18 inhibits transferrin uptake. Furthermore, SNX18 successfully compensates for SNX9 deficiency during endocytosis and vice versa. Finally, in real-time TIRF imaging, exogenously expressed SNX9 and SNX18 showed a considerable amount of colocalization and their spatiotemporal movements are indistinguishable. All of the above results lead

me to conclude that SNX18 functions in endocytosis, rather than in a distinct endosomal trafficking pathway. As discussed above, another member of the subfamily, SNX33 also functions in surface shedding and endocytosis of APP and PrPc. Therefore, SNX9, SNX18 and SNX33 seem to function as regulators of endocytosis from the plasma membrane, although their cargos would depend mostly on their distributions.

Because SNX18 interacts with N-WASP, a regulator of the actin cytoskeleton, and actin, it raises the possibility that SNX18 has a role in actin-cytoskeleton-mediated endocytosis, such as fluid-phase endocytosis, as does SNX9 (54). I also found SNX18 in circular dorsal ruffles and membrane ruffles at the cell periphery of NIH3T3 cells after treatment with platelet-derived growth factor (PDGF). In addition, knock down of SNX18 markedly inhibited the uptake of Alexa594-labeled dextran (Figure 1-14). Therefore, whether SNX18 also regulates clathrin-independent fluid-phase endocytosis (as SNX9 does) is of interest.

A recent report showed that the brain is almost devoid of all three proteins. Previous study showed that SNX9 is expressed in hippocampal neurons, where it has role in SV endocytosis (50). In situ hybridization results showed that SNX18 is also highly expressed in the brain, especially the hippocampus and cerebellum. The recent study showed that SNX18 is enriched in dendritic spines (J.P. and S.C., unpublished results). SNX33 has roles in APP shedding and endocytosis, which should occur in brain regions (52). Thus, unlikely previous reports, current and other results suggest that all three proteins are expressed in brain regions and have roles in the nervous system. Although

these different conclusions might arise from the different antibody sources or tissue preparations used, whether SNX18 and SNX33 act as regulators of synaptic-vesicle recycling, as SNX9 does, or whether they have discrete roles in the nervous system requires further investigation.

<CHAPTER 2>

Deleterious effects of soluble Aβ oligomers in the multiple steps of synaptic vesicle trafficking

INTRODUCTION

Alzheimer's disease (AD) is the most common form of neurodegenerative dementia. Its hallmarks are neurofibrillary tangles and amyloid plaques, which are due to hyperphosphorylated tau and amyloid beta (Aβ), respectively (55). Growing evidence indicates that the 42-residue amyloid beta protein plays an essential role in the pathogenesis of AD; thus, the amyloid cascade hypothesis proposes that the abnormal accumulation of Aβ inhibits synaptic function, gradually induces neurotic and glial changes, and initiates the process of neurodegeneration (21).

Early AD is characterized by memory and cognitive deficits that are caused by synaptic dysfunction; therefore, a failure of normal synaptic function is one of the earliest measurable deficits in AD (20). Although different assembly forms of Aβ may differentially affect AD pathogenesis at various stages of this disorder (56-58), recent evidence suggests that plaque numbers and insoluble Aβ level do not correlate well with the progression in the early stages of the disease (59). Instead there is good correlation between the cerebral elevation and accumulation of the soluble form of Aβ oligomers and the many aspects of early AD pathogenesis. For example, Aβ oligomers trigger various pathophysiological events associated with AD, such as alteration of synaptic plasticity by inhibiting long-term potentiation and facilitating long-term depression, the loss of dendritic spines, modulation of expression level of 2-amino-3-(5-methyl-3-oxo-1,2- oxazol-4-yl)propanoic acid (AMPA) and N-Methyl-D-aspartic acid (NMDA) receptors, and

destabilization of calcium homeostasis (29, 58, 60-63). Aβ oligomers are also known to have acute effects on synaptic function. For example, injection of soluble forms of human Aβ oligomers disrupt cognitive function in a rapid and transient manner (22). Endogenous or exogenous Aβ antibodies can restore synaptic function and reverse the acute effects of soluble Aβ oligomers on memory deficits in AD animal models (64-66).

Although the relationship between Aβ oligomers and synaptic function has been widely investigated, most of the previous studies mainly focused on the mechanisms of postsynaptic functions, but it is still unclear the specific step(s) in which Aβ causes the defects presynaptically during synaptic transmission (30, 67-71). The synaptic vesicle (SV) components are recycled in presynaptic nerve terminals through a local exo-endocytic pathway, which involves various protein–protein interactions, and recent studies have revealed some of the molecular details of these processes (12, 72). The SV pool constitutes a recycling pool, which includes a readily-releasable pool (RRP) and a reserve pool, and a resting pool that does not normally recycle. The kinetics of each of the recycling steps all play important roles in determining the efficacy of synaptic function during synaptic transmission. Therefore, uncovering the mechanisms of the above step(s) in which SV trafficking was affected by Aβ oligomers and which intracellular signaling pathways are involved may provide insight for the identification of suitable drug targets and the development of new therapeutic interventions, but these mostly remain unclear.

To reveal the effect of soluble Aβ oligomers on presynaptic function, cultured hippocampal neurons were acutely treated with nanomolar concentrations of Aβ oligomers. Using a quantitative kinetic analysis of the trafficking mechanisms of SV, I uncover the subtle alterations in the multiple steps of SV trafficking and the intracellular signaling pathways are involved, thus providing a causal relationship between Aβ oligomers and presynaptic dysfunction.

MATERIAL AND METHODS

Materials

Synthetic Aβ peptide 1-42 was from Bachem (Bubendorf, Switzerland) and anti-beta amyloid antibody (6E10) was purchased Signet™ (Dedham, MA). NuPAGE 4-12% Bis-Tris gel and Fluo-5F-AM are from Invitrogen (Grand Island, NY). Bafilomycin A1 and Roscovitine were from Calbiochem (San Diego, CA). Calpain inhibitor III, HFIP and DMSO were from Sigma (St. Louis, MO).

Aβ oligomers preparation

Synthetic Aβ peptide was dissolved to 1 mM in HFIP. The HFIP was removed by evaporation in fume hood for 2 hr followed by drying under vacuum in a SpeedVac centrifuge for 10 min at 800g. The resulting clear peptide film was stored at -20˚C. The peptide film was resuspended to 1 mM in DMSO and sonicated for 10 min using bath sonication. This DMSO solution diluted to 100 μM in cold F-12 with vortexing. Next, the solution was stored at 4 ˚C at least 12 hr and diluted into the appropriate concentration in culture medium.

Western blot analysis

For the analysis of Aβ oligomers, samples of the final dilution in the culture media were loaded onto 4-12% Bis-Tris NuPAGE gels. NuPAGE MES running buffer and transfer buffer were from Invitrogen. Samples are

transferred to PVDF membrane (BioRad, Hercules, CA). Membranes were incubated with the primary antibody 6E10 and visualized using a SuperSignal West Pico Chemiluminescent Substrate (Thermo Scientific, Rockford, IL). To verify the blocking degree of Aβ oligomers by 6E10 antibody, the Aβ peptides were pre-incubated with 6E10 antibody for 2 hr at room temperature with agitation, and immunoprecipitated with protein G sepharose beads (Amersham Biosciences, Piscataway, NJ). The samples were from 'before' and 'after' bead binding, especially 'after' were separated into supernatants and precipitates.

To measure the amount of SV protein expression level after Aβ oligomers treatment, neurons at DIV18 were washed twice with cold PBS and extracted at 4°C for 1 hr in 1 % Tx-100 buffer (10 mM Tris-HCl pH 7.4, 5 mM EDTA, 150 mM NaCl, 1% Triton X-100, 10% glycerol, 1 mM sodium orthovanadate, 1 mM PMSF, 10 mM leupeptin, 1.5 mM pepstatin, and 1 mM aprotinin). They were then clarified by centrifugation at 15,000 ***g*** for 10 min and protein concentrations were determined with a BCA protein assay reagent kit (Pierce). Samples were subjected to SDS-PAGE and transferred to a polyvinylidine difluoride membrane (Bio-Rad). The membrane was blocked with 5% skim milk in TBST (10 mM Tris-HCl, 100 mM NaCl and 0.1% Tween-20, pH 7.5) for 1 hr, washed and probed with primary antibody for 1 hr at room temperature. After extensive washing in TBST, the membrane was incubated with horseradish peroxidase (HRP)-conjugated secondary antibody (Jackson ImmunoResearch Laboratories). Proteins were visualized with enhanced chemiluminescence reagent (Amersham Biosciences).

Neuron culture and transfection

Hippocampal neurons derived from E-18 primary rats were prepared as described (73). Briefly, hippocampi were dissected, dissociated with papain, and triturated with a polished half-bore Pasteur pipette. The cells (2.5 X 10^5) in minimum Eagle's medium supplemented with 0.6% glucose, 1 mM pyruvate, 2 mM L-glutamine, 10% fetal bovine serum, and antibiotics were plated on poly-D-lysine-coated glass coverslips in a 60-mm Petri dish. Four hr after plating, the medium was replaced with basal media Eagle's (Invitrogen, San Diego, CA) supplemented with 2% B-27, 10 mM HEPES, and 0.5 mM pyruvate or Neurobasal (Invitrogen) supplemented with 2% B-27, 0.5 mM L-glutamine. 4 μM of 1-β-D-cytosine-arabinofuranoside (Ara-C, Sigma) was added as needed. Neurons were transfected using a modified calcium-phosphate method (74). Briefly, vGlut1-pHluorin (vGpH) with pU6mRFP was transfected at 10 days *in vitro*. The vGpH and pU6mRFP constructs were cotransfected in a ratio of 5:1.

vGlut1-pHluorin exo/endocytosis assay

Coverslips were mounted in a perfusion/stimulation chamber equipped with platinum-iridium field stimulus electrodes (EC-S-10, LCI, Seoul, Korea) on the stage of an Olympus IX-71 inverted microscope with 40 X, 1.0 NA oil lens. The cells were continuously perfused at room temperature with imaging buffer solution. 10 μM 6-cyano-7-nitroquinoxaline-2,3-dione was added to imaging buffer to reduce spontaneous activity and prevent recurrent excitation

during stimulation. Light emit from LED machine (LCI, Seoul, South Korea). Time-lapse images were acquired every 5 s for 4 min using a back-illuminated Andor iXon 897 EMCCD camera (512X512, 16 bit; Andor Technologies, Belfast, Northern Ireland) driven by MetaMorph. From the 4^{th} frame, the cells were stimulated (1 ms, 20-50 V, bipolar) for 600 APs at 20 Hz using an A310 Accupulser current stimulator (World Precision Instruments, Sarasota, FL). In order to measure the rate of endocytosis and exocytosis, fluorescence time course trace in the absence and presence of bafilomycin A1 were fitted with a double exponential as previously described (75). All fitting was done using individual error bars to weight the fit, using SigmaPlot 10.0. Data are presented as means ± s.e. Statistical analysis was carried out with PASW Statistics 18 (formerly SPSS Statistics). For multiple conditions, analysis of variance (ANOVA) followed by Tukey's HSD *post hoc* test was used.

Synaptic vesicle pool size measurement

To measure SV pool size, vGpH transfected neurons were stimulated with 1,800 APs at 20 Hz in the presence of 1 μM bafilomycin to trace the response. The amplitude of fluorescence increase corresponds to the recycling pool. The resting pool was uncovered by applying ammonium chloride solution for one min. Data are presented as means ± s.e. Statistical analysis was carried out with PASW Statistics 18 (formerly SPSS Statistics). For multiple conditions, analysis of variance (ANOVA) followed by Tukey's HSD *post hoc* test was used.

Regeneration rate of fusion-competent vesicles

To measure repriming kinetics, vGpH transfected neurons were stimulated with 100 APs at 50 Hz to measure the value of ΔF_1. After 10 min recovery time, neurons were stimulated with 600 APs at 50 Hz followed by the second stimulation 100 APs at 50 Hz, using different delay time (0, 10, 20, 40, 80 s) to measure ΔF_2. By dividing the fluorescence amplitude of second stimuli (ΔF_2) by that of first stimuli (ΔF_1), the time course graph of regeneration rate of fusion-competent SVs was calculated. Data are presented as means ± s.e. Statistical analysis was carried out with PASW Statistics 18 (formerly SPSS Statistics). For multiple conditions, analysis of variance (ANOVA) followed by Tukey's HSD *post hoc* test was used.

Release probability of RRP

To measure the release probability of RRP, time-lapse images of vGpH transfected neurons were acquired every 0.4 s for 30 s, stimulated with 40 APs at 20 Hz at 4^{th} frame. The amplitude of fluorescence change in 40 APs was ΔF_{40APs}. After 1 min, the second time-lapse images were acquired every 100 ms for 45 s, stimulated with 1 AP at 150^{th} frame. This time lapse images with 1 AP stimulation were repeated 10 times. The average amplitude of fluorescence change in 1 AP was ΔF_{1AP}. To get an unbiased estimate of release probability, the average ΔF response amplitude to single AP (ΔF_{1AP}) was divided by the RRP estimate (ΔF_{40APs}) for each synapse, providing the release probability of a vesicle in the RRP (P_v). The P_v distribution was fit

with a Gamma function $f(x) = Ax^{\alpha-1}e^{-\beta x}$ (76). Considering that the average number of vesicles in the RRP is 4.6 (77), the release probability at any individual synapse, P_r, is estimated following equation.

$$P_r = 1 - (1-P_v)^n$$

where P_v is the release probability for an individual vesicle and n is the number of docked vesicles. Data are presented as means ± s.e. Statistical analysis was carried out with PASW Statistics 18 (formerly SPSS Statistics). For multiple conditions, Kolmogorov-Smirnov test was used.

Recovery rate of a depleted RRP

To measure ability to recover from RRP depression, vGpH transfected neurons were stimulated with 40 APs at 20 Hz to measure ΔF_1. After variable amount of chase time (10, 20, 40, 80s), the same stimuli were applied to measure ΔF_2. By dividing the fluorescence amplitude of second stimuli (ΔF_2) by that of first stimuli (ΔF_1), the time course graph of recovery rate of depleted RRP was calculated. For multiple conditions, analysis of variance (ANOVA) followed by Tukey's HSD *post hoc* test was used.

Calcium clearance rate measurement

The cultured rat hippocampal neurons were stained with 2 μM fluo-5F-AM for 10 min at 37°C. After 10 min washing, neurons were stimulated with 300 APs at 10 Hz. Time-lapse images were acquired every 2 s for 7 min using a back-illuminated Andor iXon 897 EMCCD camera. The amplitude of

fluorescence increase corresponds to the calcium release, while the kinetics of fluorescence decrease indicates the calcium clearance rate. Data are presented as means ± s.e.

Image analysis

All of the time-lapse images were analyzed using MetaMorph software, Image J (NIH) and SigmaPlot 10.0. Synapses were identified boutons highlighting the stimulus-dependent increase in vGpH fluorescence. Square regions of interest (ROIs) were positioned at the center of exocytotic hot-spots, revealing active synapses. Photobleaching drift was corrected by fitting a double exponential function.

AD transgenic mice model

Transgenic AD model mice, 5XFAD (tg6799) overexpress both mutant human APP(695) with the Swedish (K670N, M671L), Florida (I716V), and London (V717I) Familial Alzheimer's Disease (FAD) mutations and human PS1 harboring two FAD mutations, M146L and L286V. Mice from this founder line have high APP expression correlating with high burden and accelerated accumulation of the 42 amino acid species of Aβ (Aβ-42). 5XFAD mice generate Aβ-42 almost exclusively and rapidly accumulate massive cerebral level. TG mice (tg6799) were kindly provided by Inhee Mook-Jung (Seoul National University, Seoul, South Korea). Experiments were performed in

accordance with guidelines set forth by the Seoul National University Council Directive for the proper care and use of laboratory animals.

RESULTS

The size of the functional recycling pool decreases while that of resting pool increases by Aβ oligomers treatment

To address the effect of Aβ oligomers on presynaptic function, vGlut-pHluorin (vGpH) transfected hippocampal neurons were used. vGpH is a vesicular glutamate transporter 1 fused with pHluorin, a modified GFP with high pH sensitivity (78). When targeted to the SV lumen, vGpH is quenched and upon exocytosis, the relative basic pH of the extracellular space allows the vGpH to fluoresce. Its fluorescence is again quenched once SVs are endocytosed and re-acidified; thus, it reliably reflects the kinetics of exo-endocytic trafficking of SVs. From this, it also obtained the ratio of recycling/resting pool size. At DIV18, neurons were treated for 2 hr with 200 nM of crude oligomers preparation made from synthetic Aβ peptides (Figure 2-1). This concentration of Aβ oligomers, which is lower than that typically used in neurotoxicity and cell-death studies, was found to induce no obvious cell death or changes in ATP level in the previous studies (30). Consistent with previous data, it was not induced any noticeable changes in the level of pyknotic nuclei by 2 hr exposure to 200 nM Aβ oligomers (Figure 2-1D, E).

The SV pool constitutes a recycling pool, which includes a readily-releasable pool (RRP) and a reserve pool, and a resting pool that does not normally recycle. The size of the pool of vesicles that recycle plays important roles in determining the efficacy of synaptic function during repetitive stimulation. Therefore, the effect of Aβ oligomers on the SVs pool size is

tested first. The amplitude of the response to a train of 1,800 APs at 20 Hz in the presence of bafilomycin A1, a V-type ATPase inhibitor that blocks acidification of endocytosed SVs (79), constitutes the total recycling pool. The resting pool of vesicles which are refractory to stimulation can be uncovered by adding NH_4Cl to trap all of the vesicles in an alkaline state, and hence unquench all acidic vesicles that have not released (79). As a result, Aβ oligomers induced an alteration of the recycling/resting pool ratio through an expansion of the resting fraction at the expense of the recycling fraction (recycling fraction : resting fraction = 64 ± 2.1% : 36 ± 2.1% for control, 50 ± 2.1% : 50 ± 2.1% for Aβ oligomers). Pretreatment of Aβ oligomers with the antibody 6E10, which removes Aβ *n*-oligomers from the supernatant (Figure 2-1B, C), blocked the Aβ oligomers effect (Figure 2-2).

Aβ oligomers slow down the rate of endocytosis, but not the rate of exocytosis

In order to measure the kinetics of exo/endocytosis, the neurons at DIV18 transfected with vGpH were stimulated with 600 APs at 20 Hz. After stimulation, the kinetics of the vGpH fluorescence decay was significantly slowed in boutons treated with Aβ oligomers compared to a control, reflecting a slower rate of SV endocytosis (τ = 28.38 ± 0.09 s for the control; τ = 48.99 ± 0.60 s for Aβ oligomers; see Figure 2-3). Any defect on endocytosis was observed when experiments were done using a peptide that contained the Aβ monomers (Figure 2-4). Once again, preincubation with the 6E10 blocked the

Aβ oligomers effect (Figure 2-3A, B). When Aβ oligomers-containing medium was replaced with control medium after 2 hr of treatment, the defects in endocytosis returned to normal level, demonstrating that Aβ oligomers treatment did not induce permanent damage to the neurons and the effect is reversible (Data not shown).

To test the Aβ oligomers effect on exocytosis, bafilomycin A1 was applied. The rate of exocytosis, however, was not affected by Aβ oligomers (Figure 2-3B-D), suggesting that the role of Aβ oligomers in SV recycling may be restricted to the endocytic realm. It was also found that the ratio Endo/Exo was significantly reduced when the cells were treated with Aβ oligomers (Figure 2-3E, F), thus indicating that Aβ oligomers impair SV endocytosis not only after stimulation but also during the train of action potentials. Again, Aβ monomers or preincubation with the 6E10 antibody against Aβ oligomers abolished the effect of Aβ oligomers on endocytosis during stimulation (Figure 2-3 and Figure 2-4).

The release probability of RRP is increased by treatment with Aβ oligomers

Next, it was examined whether exogenous Aβ oligomers affect the probability that each of primed SVs has fused with the membrane in response to one AP (P_v), which can be obtained by dividing the average response amplitude for a single AP with the amplitude attained with 40 APs (76). The distribution of P_v of Aβ oligomers-treated neurons and control neurons followed a γ-function

characteristic (Figure 2-5A-C). The average P_v in the Aβ oligomers-treated neurons was significantly elevated compared to the value in the control, whereas preincubation with 6E10 abrogated the effect (0.083 ± 0.003 for the control, 0.097 ± 0.005 for Aβ oligomers, 0.081 ± 0.003 for Aβ oligomers with 6E10, p = 0.029 for control and Aβ oligomers, p = 0.152 for control and Aβ oligomers with 6E10, Kolmogorov–Smirnov test). Considering that the average number of vesicles in the RRP is 4.6 (77), estimated the release probability (P_r) of the boutons is 0.328 ± 0.014 for the control, 0.374 ± 0.023 for Aβ oligomers, and 0.321 ± 0.014 for Aβ oligomers with the 6E10 (Figure 2-5D).

Regeneration of fusion-competent vesicles is severely impaired by treatment with Aβ oligomers

The observations described above left open the question of whether Aβ oligomers affect the downstream steps in the SV cycle after membrane internalization. To find out this, a test pulse (100 APs at 50 Hz) was first applied, then after 5 min recovery, 600 APs at 50 Hz was given to deplete the fusion-competent vesicles (Figure 2-6A). After a variable amount of chase time, another 100 APs at 50 Hz was applied. With more chase time, a greater number of vesicles became available for the next round of exocytosis. The regeneration of functional SVs was severely delayed in Aβ oligomers-treated neurons (Figure 2-6B). In the control, after 40 s of chase time, most of the vesicles were recycled back to the fusion-competent state ready for the next

round of exocytosis. In contrast, in the Aβ oligomers-treated neurons, there was a substantial delay in SV reformation and only 50% of the released vesicles could be recycled back even after 80 s of chase time. Preincubation with the 6E10 antibody largely attenuated, although not completely, the effect of Aβ oligomers on repriming. These results demonstrate a severe impairment of the backup of SV during recycling under these conditions, suggesting that Aβ oligomers affect one or multiple steps of the recycling pathway after vesicle membrane internalization from an endocytic vesicle to a fusion-competent vesicle.

The recovery from RRP depletion is slowed down by treatment with Aβ oligomers

The smaller recycling pool, impaired repriming, and higher release probability all favor slower recovery after synaptic depression during repetitive stimulation. Thus, it was examined whether Aβ oligomers affect the synaptic ability to recover from depression caused by the depletion of the RRP (80). The RRP was depleted by 40 APs at 20 Hz (ΔF_1), and after a variable amount of chase time ranging from 10 to 80 s, the same stimulus was applied (ΔF_2). The amplitude of fluorescence increase in each train was used to estimate the amount of SVs existed in RRP. At short intervals, ΔF_2 was depressed relative to ΔF_1 due to the depletion of the RRP. Although the magnitude of the depression measured 10 s after the first stimulus train was not different in Aβ oligomers-treated neurons and control neurons, the time constant of recovery

rate from the depression was altered (13.25 ± 1.98 s in the control neurons; 21.67 ± 25.70 s in the Aβ oligomers; see Figure 2-7). Indeed, even after an 80 s delay, a full recovery from depression was not attained in the Aβ oligomers-treated neurons. Consistently, preincubation with the 6E10 antibody against Aβ oligomers abrogated the effect (τ = 14.10 ± 1.44 s; see Figure 2-7).

Ca^{2+} clearance rate is not altered by acute Aβ oligomers treatment

Recent study suggests that cellular Ca^{2+} clearance is impaired in AD mouse model (81). In addition, the dysregulation of Ca^{2+} handling is associated with the synaptic transmission and synaptic plasticity. To test whether Ca^{2+} clearance rate is altered by acute treatment of Aβ oligomers, neurons were incubated with fluo-5F-AM for 10 min and then stimulated with 300 APs at 10 Hz. The result showed that Ca^{2+} clearance rate did not reach statistical significance between Aβ oligomers–treated neurons and control neurons. (τ = 139.23 ± 21.49 s for control, τ = 150.86 ± 16.59 s for the Aβ oligomers; see Figure 2-8A, B). The amount of residual Ca^{2+} was also not significantly altered both at 1 min and 5 min after stimulation (Figure 2-8C, D). These results indicate that the SV trafficking defects by Aβ oligomers are not because of abnormal Ca^{2+} clearance.

The expression level of synaptojanin 1 (Syj1) increases in Aβ oligomers-treated neurons

In order to verify whether SV proteins expression level was changed by Aβ oligomers treatment, cultured rat hippocampal neurons at DIV18 were treated with Aβ oligomers for 2 hr. Figure 2-9 showed that the expression level of synaptojanin 1 (Syj1) was increased 2~3 times after Aβ oligomers treatment. The Syj1 is representative 5-phosphatase that dephosphorylated the D-5 position phosphate from phosphatidylinositol (4,5)-bisphosphate (PIP_2). These results are consistent with previous study (30), which observed a decrease in the level of PIP_2 after 60 min of treatment with Aβ oligomers. The expression level of synaptophysin, another major SV protein, was not altered by treatment with Aβ oligomers. Therefore, it suggests that Aβ oligomers increase the Syj1 expression level, which subsequently decreases the PIP_2 level in neurons.

PIPkinase-γ expression prevents Aβ oligomers-induced defects in synaptic vesicle endocytosis

Recent evidence has implicated PIP_2 in Aβ oligomers-induced synaptic dysfunction (30). If PIP_2 deficiency is an important aspect of Aβ oligomers-induced synaptic dysfunction, restoring PIP_2 level may diminish or inhibit the action of this peptide. To test this hypothesis, phosphatidylinositol-4-phosphate-5-kinase type I-γ (PIPkinase-γ) was transfected in hippocampal neurons, since a previous work has shown that neurons overexpressing PIPkinase-γ have higher level of PIP_2 (31). PIPkinase-γ overexpression itself slowed down endocytosis, which is consistent with the previous findings in

that too much or too less PIP_2 level induces the defects in SV endocytosis (31, 82-83). The overexpression of PIPkinase-γ almost completely prevented the endocytic defects induced by Aβ oligomers. The result suggests that PIPkinase-γ expression may compensate for the decrease in the PIP_2 level after Aβ oligomers treatment thus, restoring the defects in endocytosis by Aβ oligomers (Figure 2-10A, B). The overexpression of PIPkinase-γ, however, failed to restore the pool size alteration by Aβ oligomers and further reduced the recycling pool fraction, suggesting that PIP_2 deficiency is not attributed to Aβ oligomers-induced pool size alteration and other downstream pathway(s) may be involved (Figure 2-10C).

The deleterious effect of Aβ oligomers in endocytosis was further verified using cultured hippocampal neurons derived from AD transgenic mice 5XFAD (tg6799). The 5XFAD mouse has high amyloid precursor protein (APP) expression correlating with high burden and accelerated accumulation of the 42 amino acid species of Aβ (84). Consistent with the results from exogenous Aβ oligomers treatment, endocytosis was significantly slowed in boutons derived from the 5XFAD mouse ($\tau = 18.62 \pm 0.28$ s for control, $\tau = 41.51 \pm 0.29$ s for the 5XFAD mouse; see Figure 2-11).

CDK5 inhibition by calpain inhibitor prevents Aβ oligomers-induced alteration in synaptic vesicle pool size

Recent study implicated CDK5 as a major control point for the pool size regulation of SVs (85). Since Aβ oligomers are well known to activate CDK5

activity through activating calpain and findings from AD brain samples also show an elevated CDK5 activity that supports the activation of CDK5 (86-87), whether alteration of the pool size by Aβ oligomers are mediated through calpain-CDK5 pathway was tested.

Considering that Aβ oligomers are known to activate calpain and calpain cleaves p35 to produce p25 that excessively activates CDK5, it was speculated that p35 cleavage by calpain may be involved in the Aβ oligomers-induced alteration of the pool size. Calpain inhibitor III itself had no effect on the vesicle pool size, but it completely prevented the alteration of the vesicle pool size by Aβ oligomers (recycling fraction : resting fraction = 62 ± 2.2% : 38 ± 2.2% for control, 63 ± 3.4% : 37 ± 3.4% for calpain inhibitor, 50 ± 2.1% : 50 ± 2.1% for Aβ oligomers, 63 ± 2.2% : 37 ± 2.2% for Aβ oligomers with calpain inhibitor; see Figure 2-12). These results suggest that calapin-CDK5 is implicated in the Aβ oligomers-induced alteration of pool size.

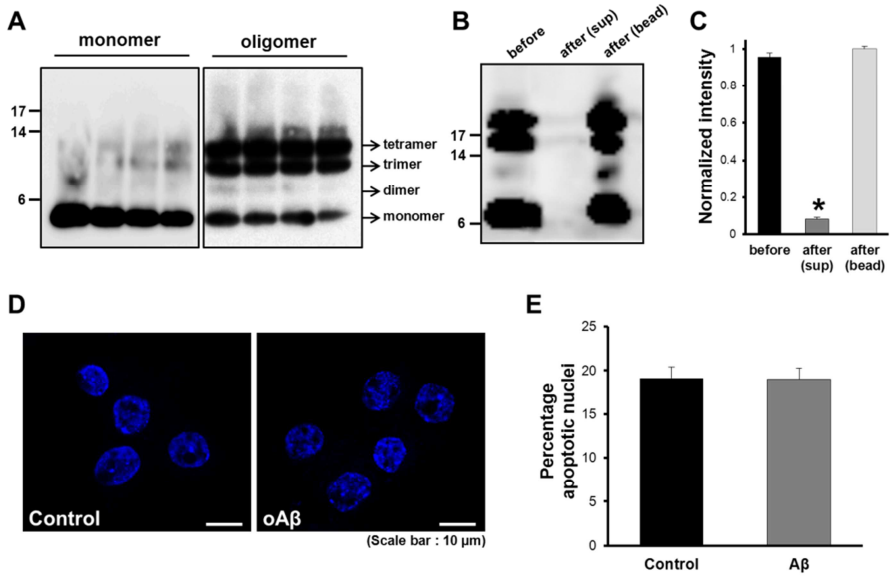

Figure 2-1. Aβ oligomers do not affect cell viability.

(A) The synthetic Aβ oligomers and Aβ monomers were analyzed by immunoblotting with anti-Aβ antibody, 6E10, following gel electrophoresis through a 4~12% Bis-Tris NuPAGE gel. In Aβ oligomers, the major bands were tetramer and trimer with slight dimer and monomer while Aβ monomers had strong monomer band and slight tetramer band. **(B, C)** Synthetic Aβ oligomers were incubated with 6E10 antibody for 2 hr at room temperature, then immunoprecipitated with protein G sepharose bead. After 2 hr incubation, the supernatants and the precipitates were separately collected and run through a 4~12% Bis-Tris NuPAGE gel. Note that "after bead binding", most of low-*n* oligomers of Aβ were disappeared, indicating that 6E10 antibody successfully immunoprecipitates low-*n* oligomers of Aβ and removes from the

supernatants. Error bars represent s.e.m. * $p < 0.01$ (ANOVA and Tukey's HSD *post hoc* test). **(D)** The cultured hippocampal neurons were treated with Aβ oligomers for 2 hr, and then stained with DAPI for measuring the level of pyknotic nuclei. Confocal micrographs of non-pyknotic nuclei in control and Aβ oligomers-treated neurons. Scale bar = 10 μm. **(E)** Quantification of the percentage of pyknotic nuclei in hippocampal neurons in control or exposed to Aβ oligomers for 2 hr (n=489 cells for control, n=265 cells for Aβ oligomers, p=0.9641). Note that acute treatment of Aβ oligomers was not induced cell death. *Statistically significant at $P<0.05$, Student's *t*-test.

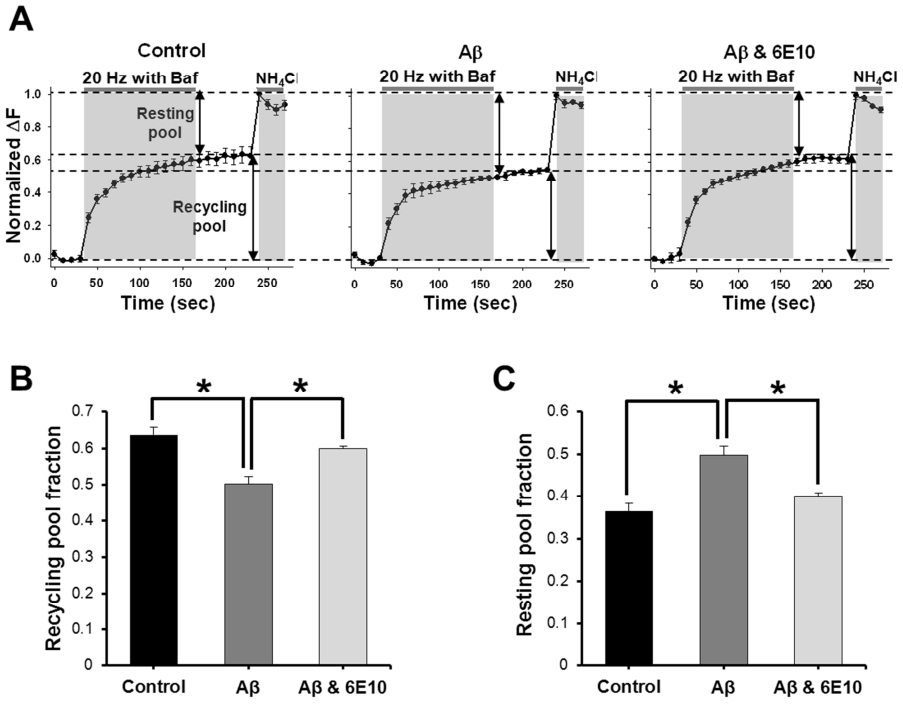

Figure 2-2. The ratio of recycling pool and resting pool of synaptic vesicle is altered by treatment with Aβ oligomers.

(A) Neurons expressing vGpH and pU6mRFP were treated with buffer, Aβ oligomers or Aβ oligomers with 6E10 antibody for 2 hr. And then neurons were stimulated with 1800 APs at 20 Hz in the presence of bafilomycin A1. The plateau in fluorescence reflects the entire recycling pool. All remaining acidic vesicles are alkalized by NH_4Cl treatment, revealing the size of the resting pool. Fluorescence intensity was normalized to the maximum fluorescence change at NH_4Cl treatment. **(B)** Average fraction of recycling

pool in control, Aβ oligomers or Aβ oligomers with 6E10 antibody. (64% ± 2.1% for control; 50% ± 2.1% for Aβ oligomers; 60% ± 0.6 % for Aβ oligomers with 6E10). **(C)** Average fraction of resting pool in control, Aβ oligomers or Aβ oligomers with 6E10 antibody. (36% ± 2.1% for control; 50% ± 2.1% for Aβ oligomers; 40% ± 0.6 % for Aβ oligomers with 6E10). Data are presented as means ± s.e. * $p < 0.01$ (ANOVA and Tukey's HSD *post hoc* test).

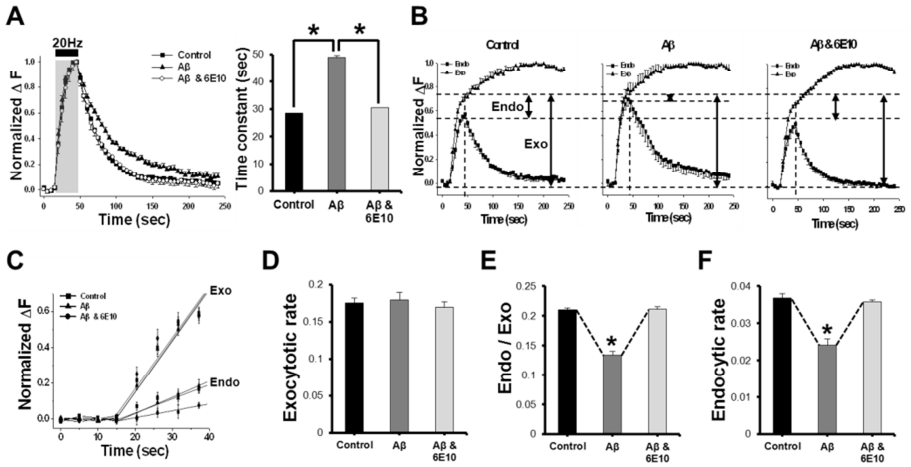

Figure 2-3. Aβ oligomers impair endocytosis, not exocytosis.

(A) Normalized vGpH fluorescence intensity profiles of the boutons from each condition after stimulation (n = 6). The decay of vGpH fitted by a double exponential with $\tau = 28.38 \pm 0.09$ s for the control; $\tau = 48.99 \pm 0.60$ s for Aβ oligomers; and $\tau = 30.50 \pm 0.07$ s for Aβ oligomers with 6E10 antibody. **(B)** 1,800APs were given in the presence of bafilomycin A1 to measure exocytosis exclusively. Endocytosis during the stimulation was derived by subtracting the vGpH fluorescence in the absence of bafilomycin from that in the presence of bafilomycin. The fluorescence values were normalized to the peak fluorescence change. **(C-F)** The rate of exocytosis/endocytosis was obtained by linear fits to the first 300 AP train. Data are presented as means ± s.e. * $p < 0.01$ (ANOVA and Tukey's HSD *post hoc* test).

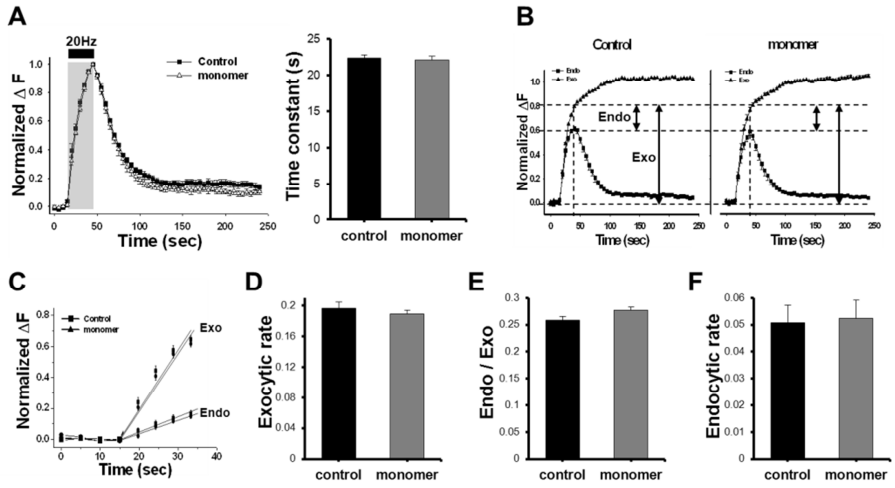

Figure 2-4. Aβ monomers do not impair endocytosis and exocytosis both during and after stimulation.

(A) Normalized vGpH fluorescence intensity profiles of the boutons from each condition after stimulation (n = 7-8 per group). The decay of vGpH fitted by a double exponential with $\tau = 22.34 \pm 0.45$ s for the control and $\tau = 22.10 \pm 0.48$ s for Aβ monomer. **(B)** 1,800 APs were given in the presence of bafilomycin A1 to measure exocytosis exclusively. Endocytosis during the stimulation was derived by subtracting the vGpH fluorescence in the absence of bafilomycin from that in the presence of bafilomycin. The fluorescence values were normalized to the peak fluorescence change. **(C-F)** The rate of exocytosis/endocytosis was obtained by linear fits to the first 300 AP train. These results suggested that Aβ monomers are not different with control. * p=0.9407 (unpaired *t*-test).

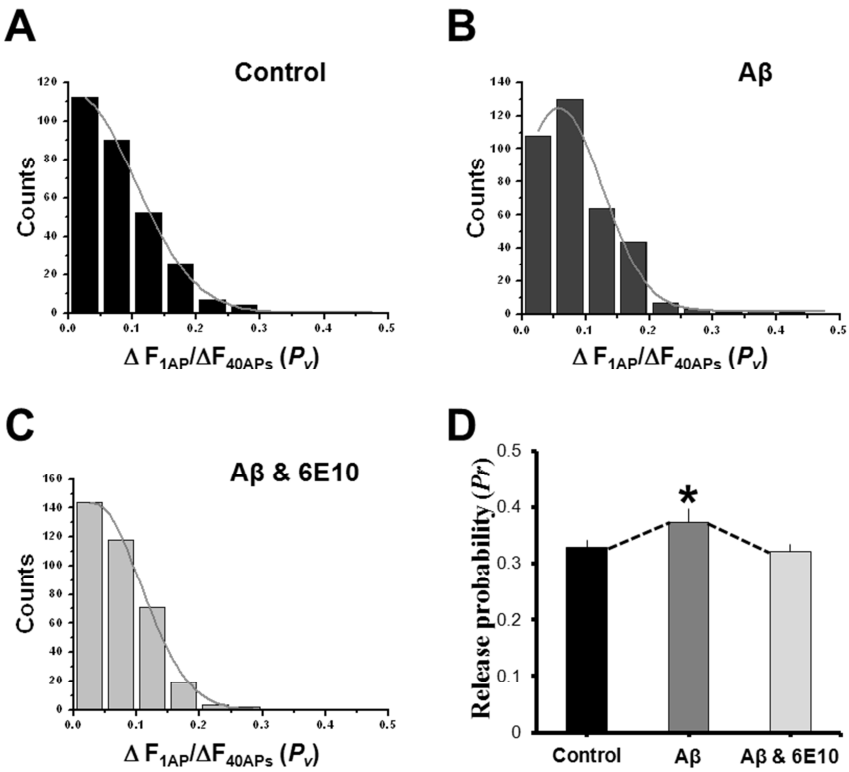

Figure 2-5. Aβ oligomers increase the release probability of readily releasable pool (RRP).

(A-C) The histograms of intrinsic release probabilities from boutons of control (**A**), Aβ oligomers (**B**) and Aβ oligomers-treated neurons with 6E10 antibody (**C**). The ratio between a single AP (ΔF_{1APs}) and 40 APs (ΔF_{40APs}) provides the intrinsic release probability of a vesicle in the RRP. **(D)** Continuous grey line is a γ distribution with shape parameter constrained to 2, giving the scale parameter 0.0328 ± 0.014 for control, 0.0374 ± 0.023 for Aβ oligomers and 0.0321 ± 0.014 for Aβ oligomers with 6E10 antibody. It is judged by Kolmogorov-Smirnov test (p = 0.029 for control and Aβ oligomers, p = 0.152 for control and Aβ oligomers with 6E10).

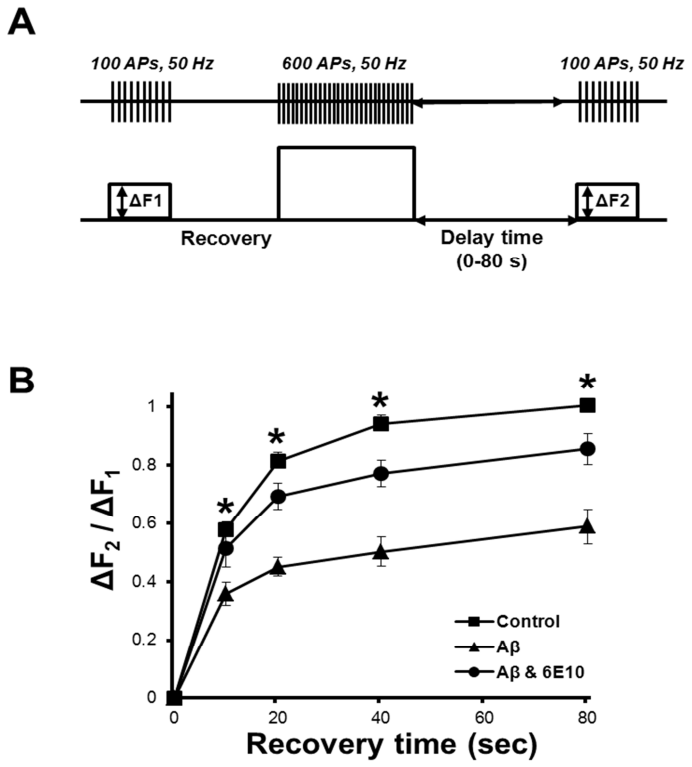

Figure 2-6. Regeneration of fusion-competent vesicle is severely impaired by treatment with Aβ oligomers.

(A) Protocol for measuring repriming rate. Neurons cotransfected with vGpH and pU6mRFP were treated with buffer (square), Aβ oligomers (triangle) or Aβ oligomers with 6E10 antibody (circle) for 2 hr. It was first stimulated with 100 APs at 50 Hz (ΔF_1). After 5 min recovery time, neurons were stimulated with 600 APs at 50 Hz to deplete all recycling pool. After variable chase time (0 to 80s), neurons were stimulated again with 100 APs at 50 Hz (ΔF_2). **(B)** Normalized ratio of $\Delta F_2/\Delta F_1$ profiles of the boutons from control (square), Aβ oligomers (triangle) and Aβ oligomers with 6E10 antibody (circle). Data are presented as means ± s.e. * $p < 0.01$ (ANOVA and Tukey's HSD *post hoc* test).

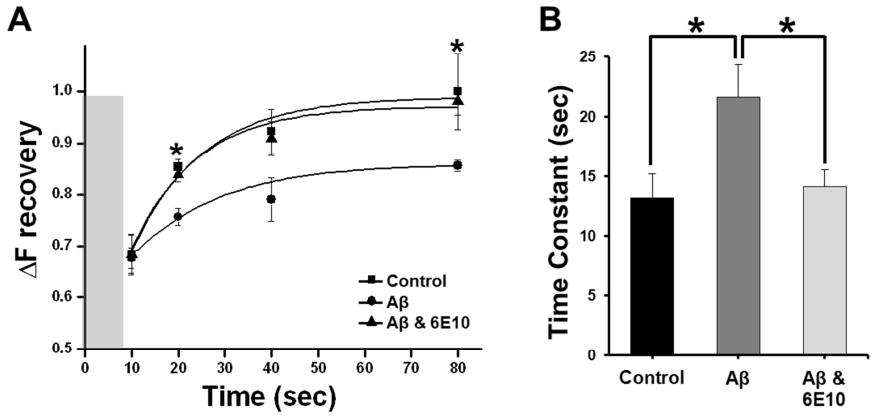

Figure 2-7. The recovery rate of depleted RRP is defected by treatment with Aβ oligomers.

(A) The time course graph of ΔF recovery of the depleted RRP from control (square), Aβ oligomers (triangle) or Aβ oligomers-treated neurons with 6E10 antibody (circle). The ΔF recovery was obtained from the response to first 40 AP at 20 Hz stimulation (ΔF_1) is divided by that of second 40 APs at 20 Hz stimulation (ΔF_2). The second stimulation was started at 10, 20, 40 and 80s after the first stimulation. Continuous lines are single exponential curve fits to the data, respectively. **(B)** Time constants from single exponential fits in (A) are 13.25 ± 1.98 s for control; 21.67 ± 2.70 s for Aβ oligomers; 14.10 ± 1.44 s for Aβ oligomers with 6E10 antibody. Data are presented as means ± s.e. * $p < 0.01$ (ANOVA and Tukey's HSD *post hoc* test).

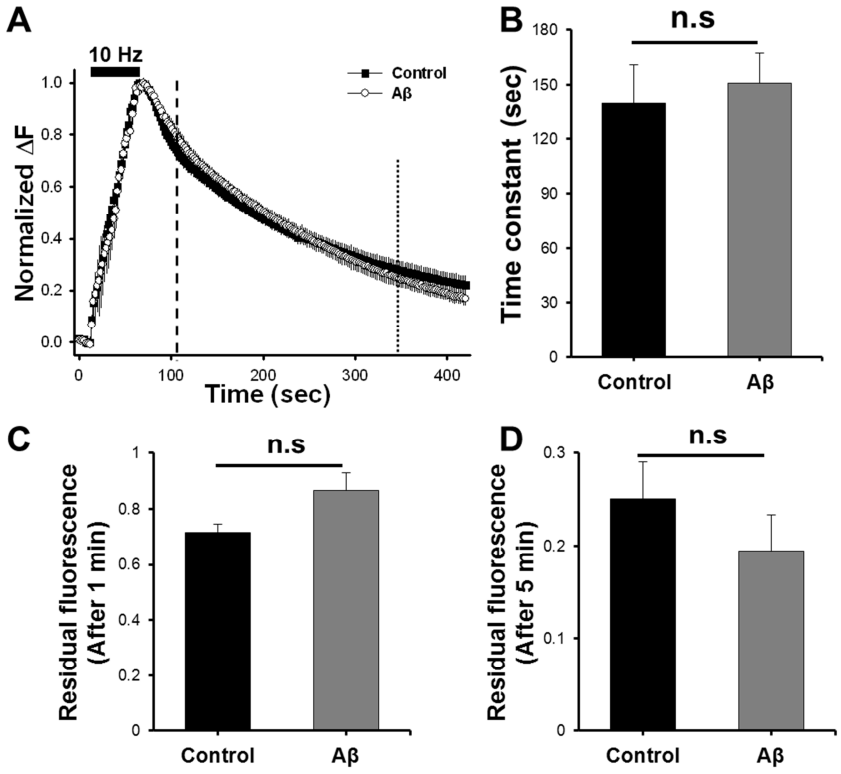

Figure 2-8. Ca^{2+} clearance rate is not altered by acute Aβ oligomers treatment.

(A) Hippocampal neurons were treated with buffer or Aβ oligomers for 2 hr. After incubation with fluo-5F-AM for 10 min, the neurons were stimulated with 300 APs at 10 Hz. **(B)** Time constant of calcium clearance in control and Aβ oligomers treatment. Note that the calcium clearance rate was not changed by Aβ oligomers treatment. Also, after 1 min **(C)** or 5 min **(D)** later from stimulation, residual calcium was not distinguishable between control and Aβ oligomers-treated neurons. * 'n.s.' stands for 'not significant'.

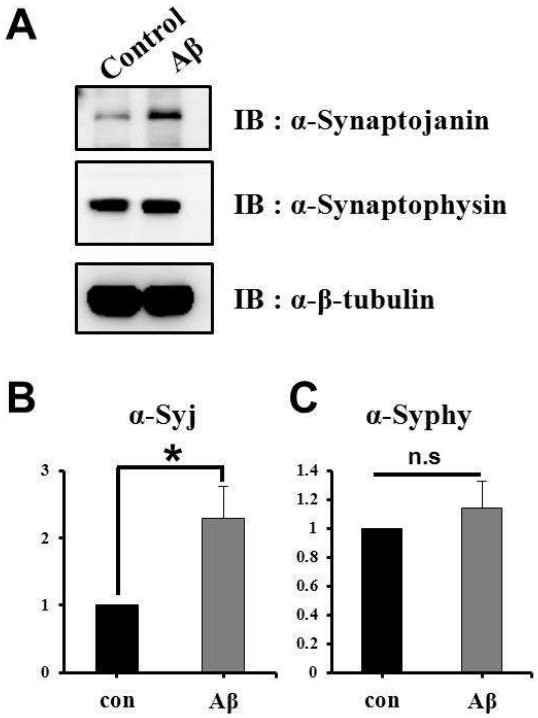

Figure 2-9. The expression of synaptojanin but not synaptophysin is increased by acute Aβ oligomers treatment.

(A) Western blot analysis of synaptojanin, synaptophysin and β-tubulin in without or with Aβ oligomers treatment from rat hippocampal neurons at DIV18. **(B)** Quantitative analysis of the blot in (A). Note that the expression level of synaptojanin significantly increased after Aβ oligomers treatment. The level of synaptophysin was unaffected by the Aβ oligomers (n=8). *Statistically significant at $P<0.05$, Student's *t*-test.

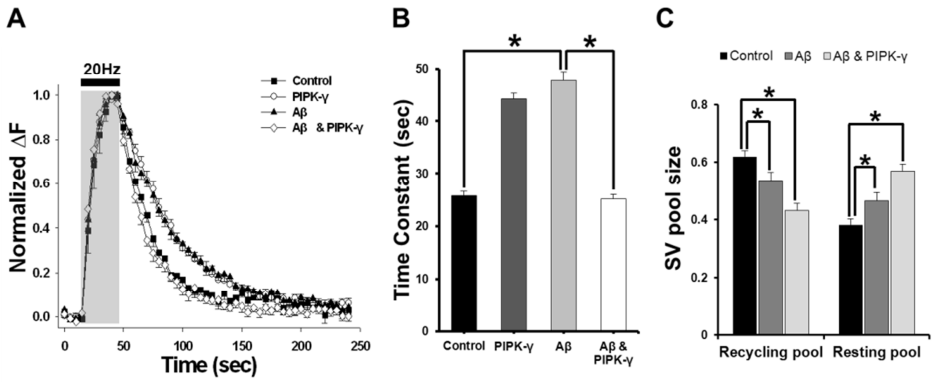

Figure 2-10. PIPkinase-γ expression prevents Aβ oligomers-induced defects in synaptic vesicle endocytosis but does not prevent an alteration of the SV pool size.

Neurons were triply transfected with vGpH, pU6mRFP and HA empty vector or HA-PIPkinase-γ at DIV10 and carry out endocytosis assay at DIV17-18. The 200 nM Aβ oligomers were treated for 2 hr. **(A)** Normalized vGpH fluorescence intensity profiles of the boutons from control (square), PIPkinase-γ (circle), Aβ oligomers (triangle) and Aβ oligomers and PIPkinase-γ (diamond) which were stimulated with 600 APs at 20 Hz. Average fluorescence intensity profiles were plotted as $\Delta F/F_0$ against time. **(B)** The decay of vGpH fluorescence was fitted by a double exponential with τ = 25.70 ± 0.85 s for control; τ = 44.27 ± 1.03 s for PIPkinase-γ; τ = 47.80 ± 1.62 s for Aβ oligomers; τ = 25.14 ± 0.81 s Aβ oligomers and PIPkinase-γ. Data are presented as means ± s.e. * $p < 0.01$ (ANOVA and Tukey's HSD *post hoc* test).

(C) Neurons were stimulated with 1,800 APs at 20 Hz in the presence of bafilomycin A1. Fluorescence intensity was normalized to the maximum fluorescence change at NH_4Cl treatment. Average fraction values of recycling and resting pools in control, Aβ oligomers or Aβ oligomers with PIPkinase-γ (recycling fraction : 63% ± 2.7% for control; 56% ± 2.1% for Aβ oligomers; 51% ± 3.2% for Aβ oligomers with PIPkinase-γ). Data are presented as means ± s.e. * $p < 0.01$ (ANOVA and Tukey's HSD *post hoc* test).

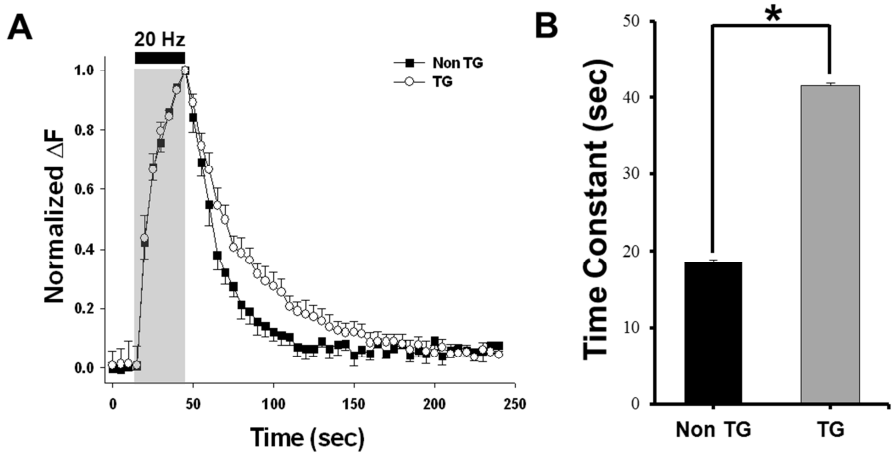

Figure 2-11. The hippocampal neurons derived from AD transgenic mice 5XFAD (tg6799) also show delayed endocytosis.

Hippocampal neurons from non-transgenic or AD transgenic mouse (tg6799) were cotransfected with vGpH and pU6mRFP at DIV10 and carry out endocytosis assay at DIV17-18. **(A)** Normalized vGpH fluorescence intensity profiles of the boutons from non-transgenic (Non-TG, square) and AD transgenic mice (TG, circle) which were stimulated with 600 APs at 20 Hz. Average fluorescence intensity profiles were plotted as $\Delta F/F_0$ against time. 3 to 4 neurons were selected in each independent experiment and 30 to 40 boutons from a single neuron were analyzed. **(B)** The decay of vGpH fluorescence was fitted by a double exponential with $\tau = 18.63 \pm 0.28$ s for Non-TG; $\tau = 41.51 \pm 0.29$ s for AD TG mice. Data are presented as means ± s.e. * $p < 0.01$.

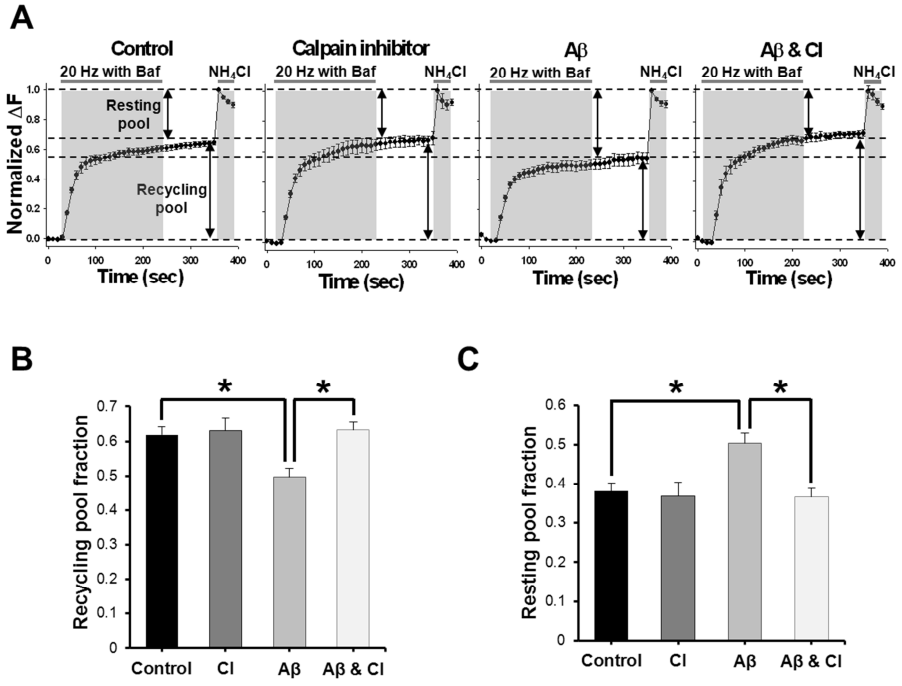

Figure 2-12. The alteration of the SV pool size by Aβ oligomers is abolished by calpain inhibition.

(A) Neurons expressing vGpH and pU6mRFP were treated with buffer, calpain inhibitor III (CI), Aβ oligomers or Aβ oligomers with CI for 2 hr. **(B, C)** Average fraction of recycling and resting pools in the control, calpain inhibitor III (CI), Aβ oligomers or Aβ oligomers with CI (recycling fraction : 62% ± 2.2% for the control; 63% ± 3.4% for CI; 50% ± 2.6% for Aβ oligomers; and 63% ± 2.1 % for Aβ oligomers with CI). Data are presented as means ± s.e. * $p < 0.01$ (ANOVA and Tukey's HSD *post hoc* test).

DISCUSSIONS

A number of different postsynaptic mechanisms, including dendritic spine loss, alteration of the AMPA and NMDA glutamate receptor numbers, and depolymerization of the actin cytoskeleton, have been identified as being involved in Aβ-induced synaptic dysfunction (23, 29, 62). The association of Aβ oligomers and presynaptic function, however, has not been firmly established. Moreover, the application of Aβ oligomers has generated contradictory results in presynaptic function (67-71, 88). Aβ oligomers injection to the presynaptic terminal of a squid giant axon inhibited synaptic transmission without affecting clathrin-coated vesicles (69) while another report showed that Aβ oligomers induce dynamin-1 depletion in hippocampal neurons, and thus disrupts SV endocytosis (88). It was also found that endogenously released Aβ oligomers positively regulate the release probability of synapses, but does not alter postsynaptic function or intrinsic neuronal excitability (67) while others reported that Aβ oligomers induce the concurrent alteration in both presynaptic and postsynaptic mechanisms (68) or it suppresses synaptic activity by inhibiting calcium currents (70). Nevertheless, all of the above results raise the possibility that Aβ oligomers have a distinct effect on presynaptic terminals in addition to its well-known effect on postsynaptic function.

The data reported here demonstrated that synthetic nanomolar concentrations of Aβ oligomers cause defects in multiple presynaptic functions. Aβ oligomers treatment slowed down the rate of endocytosis during

as well as after stimulation, although the exocytosis rate was not affected. The repriming of the SV was also severely impaired. The total SV pool was not changed, although the recycling pool size decreased with a concomitant increase in the resting pool size. The release probability of RRP was slightly but significantly increased, while recovery rate of the depleted RRP was decreased in Aβ oligomers-treated neurons. Therefore, the current study convincingly proved that Aβ oligomers act on multiple steps of SV trafficking and its signaling pathways in presynaptic terminals, which affect the efficacy of SV recycling, lead gradually to the synaptic dysfunction associated with AD.

Recent finding showed that Aβ oligomers decrease the level of PIP_2, a phospholipid that regulates key aspects of neuronal function, linking AD and phosphoinositide metabolism (30). They found that Aβ oligomers-induced PIP_2 reduction is phospholipase C (PLC) dependent. Aβ oligomers activate the PLC pathway, which decreases PIP_2 level at the plasma membrane while increasing the DAG and IP3 level. It subsequently increases intracellular Ca^{2+} concentrations in the cytosol and promotes PKC activation in Aβ oligomers-treated hippocampal neurons (30). CDK5 is also known to be activated by Aβ exposure. CDK5 is a neuronal specific cyclin-dependent kinase; Aβ exposure induces cleavage of p35 into p25 by calpain, and activates CDK5, which increases phosphorylation of pathological substrates (86, 89).

The current study demonstrated that Aβ oligomers affect both downstream pathways; PIP_2 and calpain-CDK5. Endocytic defects were prevented by PIPkinase-γ expression, suggesting that PIPkinase-γ expression may

compensate for the decrease in the PIP_2 level after Aβ oligomers treatment thus, restoring the defects in endocytosis by Aβ oligomers. Alteration in the pool size was prevented by calpain inhibitor III. Recent study reported that access to the resting pool is determined by the balance of CDK5 and calcineurin activities, and that dynamic control of this balance could provide a potent control system for tuning synaptic performance (85). Since the expression of calcineurin is known to be downregulated in Aβ oligomers-treated neurons and AD patient brains (90), calcineurin-mediated pathway also may play a role in pool size alteration by Aβ oligomers treatment.

The ability of either PIP_2 or calpain-CDK5 to mitigate the Aβ oligomers defects of SV trafficking could be the result of an independent effect, as PIPkinase-γ expression failed to restore pool size alteration. These results suggest that PIP_2 and/or calpain-CDK5 are involved in the Aβ oligomers-induced defects of SV trafficking. These results identify presynaptic pathways involved in this process that may be relevant to the early pathogenesis of AD. This data not only support the hypothesis that soluble, low-*n* oligomers of Aβ induce synaptic dysfunction that could lead to cognitive impairment in AD patients, but also identify PIP_2 and calpain-CDK5 as downstream effectors of Aβ oligomers-induced presynaptic dysfunction. Thus, combinational treatments targeting these pathways could be promising therapeutic options for the treatment or prevention of synaptic dysfunction in early AD.

GENERAL DISCUSSION

The current studies demonstrated that SNX18 functions in CME, sharing a redundant role with SNX9, and soluble Aβ oligomers induce a number of defects in CME process of SVs in neurons.

Vertebrate genomes express three proteins that are closely related: SNX9, SNX18 and SNX33 (18). These three proteins have the same domain structures; an N-terminal SH3 domain, LC and PX domains in the middle, and a C-terminal BAR domain (18). SNX9 is a well-known protein as a key regulator of vesicle trafficking during CME process (14), which infers that SNX18 may also have roles in endocytosis at the plasma membrane. A recent study, however, showed that SNX18 participates in membrane remodeling at endosomes together with AP-1 and PACS1, rather than functioning in endocytosis at the plasma membrane (18).

Contrary to the previous report, however, the current results clearly proved that SNX18 plays a role in endocytic pathways at the plasma membrane. SNX18 interacts with most of binding partners of SNX9, including N-WASP, synaptojanin and dynamin. SNX18 forms heterodimer with SNX9 at the membranous tubules and recruits dynamin to the plasma membrane, where it stimulates dynamin's GTPase activity. SNX18 successfully compensates for SNX9 deficiency during endocytosis. All of the above results support the conclusion that SNX18 functions in endocytosis at the plasma membrane, rather than in a distinct endosomal trafficking pathway.

Recently, it was reported that SNX9 regulates the amyloid precursor protein (APP) endocytosis (52), which is important step for toxic Aβ oligomers formation. Since SNX18 shares a redundant role with SNX9 in CME process, it is highly likely that SNX18 also plays a role in APP endocytosis, thus affecting Aβ oligomers production. In addition, SNX18 is found to be enriched in dendritic spines of the neurons (J.P. and S.C., unpublished results), suggesting that SNX18 may function in neuronal CME process. Indeed, a recent study showed that SNX33, another closely related sorting nexin protein to SNX18 (18), regulates APP and PrPc (cellular prion protein) endocytosis at the plasma membrane (52-53). All of these reports imply that SNX18 may play in endocytosis of APP and PrPc at the plasma membrane.

The second part of this dissertation, the effects of Aβ oligomers on CME process in neurons was studied. The data reported here indicated that acute treatment of Aβ oligomers cause defects in multiple steps of presynaptic CME process. Aβ oligomers treatment induces the alterations in the endocytic rate, the repriming rate, the SV pool composition, the release probability of RRP, and recovery rate of depleted RRP. I further found that the level of PIP_2 and calpain-CDK5 are the major targets affected by Aβ oligomers to cause the defects in CME process (30, 86). The ability of either PIP_2 or calpain-CDK5 to mitigate the Aβ oligomers defects of SV trafficking could be the result of an independent effect. Therefore, this data not only support the hypothesis that soluble, low-*n* oligomers of Aβ induce synaptic dysfunction that could lead to cognitive impairment in AD patients, but also identify PIP_2 and

calpain-CDK5 as downstream effectors of Aβ oligomers-induced presynaptic dysfunction.

According to previous data, SNX9 increases the kinase activity of phosphatidylinositol 4-phosphate 5-kinase-α (PIPkinase-α) and PIPkinase-β through interaction with them via its PX domain, and subsequently increases PIP_2 level in the plasma membrane (14). It is highly probable when considering the redundant role of SNX18 with SNX9 that SNX18 also activates PIPkinase activity, thus increases PIP_2 levels. A recent study and the current study found that Aβ oligomers decrease the PIP_2 level at the plasma membrane (30). Thus, the levels of PIP_2 is the key determinant that regulates CME process, in which SNX18 and Aβ oligomers play a positive and negative role, respectively.

From all of the above results, I concluded that SNX18 plays on key steps of CME process and Aβ oligomers affect various steps of CME process, where SNX18 is critical involved. These results raise the possibility in that CME process is tightly regulated by many critical proteins including SNX18, and any defects during CME process could result in synaptic dysfunction that is observed in many neurodegenerative diseases including AD. Therefore, the combinational treatments targeting these CME pathways could be promising therapeutic options for the treatment or prevention of synaptic dysfunction in early AD.

REFERENCE

1. Takei K, Haucke V. Clathrin-mediated endocytosis: membrane factors pull the trigger. Trends Cell Biol 2001;11(9):385-391.

2. Schmid EM, Ford MG, Burtey A, Praefcke GJ, Peak-Chew SY, Mills IG, et al. Role of the AP2 beta-appendage hub in recruiting partners for clathrin-coated vesicle assembly. PLoS Biol 2006;4(9):e262.

3. Schmid EM, McMahon HT. Integrating molecular and network biology to decode endocytosis. Nature 2007;448(7156):883-888.

4. Masuda M, Takeda S, Sone M, Ohki T, Mori H, Kamioka Y, et al. Endophilin BAR domain drives membrane curvature by two newly identified structure-based mechanisms. EMBO J 2006;25(12):2889-2897.

5. Peter BJ, Kent HM, Mills IG, Vallis Y, Butler PJ, Evans PR, et al. BAR domains as sensors of membrane curvature: the amphiphysin BAR structure. Science 2004;303(5657):495-499.

6. Takei K, Slepnev VI, Haucke V, De Camilli P. Functional partnership between amphiphysin and dynamin in clathrin-mediated endocytosis. Nat Cell Biol 1999;1(1):33-39.

7. Itoh T, Erdmann KS, Roux A, Habermann B, Werner H, De Camilli P. Dynamin and the actin cytoskeleton cooperatively regulate plasma membrane invagination by BAR and F-BAR proteins. Dev cell 2005;9(6):791-804.

8. Praefcke GJ, McMahon HT. The dynamin superfamily: universal membrane tubulation and fission molecules? Nat Rev Mol Cell Biol 2004;5(2):133-147.

9. Roux A, Uyhazi K, Frost A, De Camilli P. GTP-dependent twisting of dynamin implicates constriction and tension in membrane fission. Nature 2006;441(7092):528-531.

10. Farsad K, Ringstad N, Takei K, Floyd SR, Rose K, De Camilli P. Generation of high curvature membranes mediated by direct endophilin bilayer interactions. J Cell Biol 2001;155(2):193-200.

11. Cousin MA, Robinson PJ. The dephosphins: dephosphorylation by calcineurin triggers synaptic vesicle endocytosis. Trends Neurosci 2001;24(11):659-665.

12. Dittman J, Ryan TA. Molecular circuitry of endocytosis at nerve terminals. Annu Rev Cell Dev Biol 2009;25:133-160.

13. Evergren E, Gad H, Walther K, Sundborger A, Tomilin N, Shupliakov O. Intersectin is a negative regulator of dynamin recruitment to the synaptic endocytic zone in the central synapse. J Neurosci 2007;27(2):379-390.

14. Shin N, Ahn N, Chang-Ileto B, Park J, Takei K, Ahn SG, et al. SNX9 regulates tubular invagination of the plasma membrane through interaction with actin cytoskeleton and dynamin 2. J Cell Sci 2008;121(Pt 8):1252-1263.

15. Dawson JC, Legg JA, Machesky LM. Bar domain proteins: a role in tubulation, scission and actin assembly in clathrin-mediated endocytosis. Trends Cell Biol 2006;16(10):493-498.

16. Tsujita K, Suetsugu S, Sasaki N, Furutani M, Oikawa T, Takenawa T. Coordination between the actin cytoskeleton and membrane deformation by a novel membrane tubulation domain of PCH proteins is involved in endocytosis. J Cell Biol 2006;172(2):269-279.

17. Soulet F, Yarar D, Leonard M, Schmid SL. SNX9 regulates dynamin assembly and is required for efficient clathrin-mediated endocytosis. Mol Biol Cell 2005;16(4):2058-2067.

18. Haberg K, Lundmark R, Carlsson SR. SNX18 is an SNX9 paralog that acts as a membrane tubulator in AP-1-positive endosomal trafficking. J Cell Sci 2008;121(Pt 9):1495-1505.

19. Jolles J, Bothmer J, Markerink M, Ravid R. Reduced phosphatidylinositol kinase activity in Alzheimer's disease: effects of age and onset. Dementia 1993;4(2):81-86.

20. Selkoe DJ. Alzheimer's disease is a synaptic failure. Science 2002;298(5594):789-791.

21. Hardy J, Selkoe DJ. The amyloid hypothesis of Alzheimer's disease: progress and problems on the road to therapeutics. Science 2002;297(5580):353-356.

22. Cleary JP, Walsh DM, Hofmeister JJ, Shankar GM, Kuskowski MA, Selkoe DJ, et al. Natural oligomers of the amyloid-beta protein specifically disrupt cognitive function. Nat Neurosci 2005;8(1):79-84.

23. Palop JJ, Mucke L. Amyloid-beta-induced neuronal dysfunction in Alzheimer's disease: from synapses toward neural networks. Nat Neurosci 2010;13(7):812-818.

24. Selkoe DJ. Soluble oligomers of the amyloid beta-protein impair synaptic plasticity and behavior. Behav Brain Res 2008;192(1):106-113.

25. Benilova I, Karran E, De Strooper B. The toxic Abeta oligomer and Alzheimer's disease: an emperor in need of clothes. Nat Neurosci 2012;15(3):349-357.

26. Sivanesan S, Tan A, Rajadas J. Pathogenesis of Abeta Oligomers in Synaptic Failure. Curr Alzheimer Res 2012.

27. Li S, Hong S, Shepardson NE, Walsh DM, Shankar GM, Selkoe D. Soluble oligomers of amyloid Beta protein facilitate hippocampal long-term depression by disrupting neuronal glutamate uptake. Neuron 2009;62(6):788-801.

28. Townsend M, Shankar GM, Mehta T, Walsh DM, Selkoe DJ. Effects of secreted oligomers of amyloid beta-protein on hippocampal synaptic plasticity: a potent role for trimers. J Physiol 2006;572(Pt 2):477-492.

29. Shankar GM, Bloodgood BL, Townsend M, Walsh DM, Selkoe DJ, Sabatini BL. Natural oligomers of the Alzheimer amyloid-beta protein induce reversible synapse loss by modulating an NMDA-type glutamate receptor-dependent signaling pathway. J Neurosci 2007;27(11):2866-2875.

30. Berman DE, Dall'Armi C, Voronov SV, McIntire LB, Zhang H, Moore AZ, et al. Oligomeric amyloid-beta peptide disrupts phosphatidylinositol-4,5-bisphosphate metabolism. Nat Neurosci 2008;11(5):547-554.

31. Kim S, Kim H, Chang B, Ahn N, Hwang S, Di Paolo G, et al. Regulation of transferrin recycling kinetics by PtdIns[4,5]P2 availability. FASEB J 2006;20(13):2399-2401.

32. Farsad K, De Camilli P. Mechanisms of membrane deformation. Curr Opin Cell Biol 2003;15(4):372-381.

33. Itoh T, De Camilli P. BAR, F-BAR (EFC) and ENTH/ANTH domains in the regulation of membrane-cytosol interfaces and membrane curvature. Biochim Biophys Acta 2006;1761(8):897-912.

34. Habermann B. The BAR-domain family of proteins: a case of bending and binding? EMBO Rep 2004;5(3):250-255.

35. Weissenhorn W. Crystal structure of the endophilin-A1 BAR domain. J Mol Biol 2005;351(3):653-661.

36. Hill E, van Der Kaay J, Downes CP, Smythe E. The role of dynamin and its binding partners in coated pit invagination and scission. J Cell Biol 2001;152(2):309-323.

37. Kim Y, Kim S, Lee S, Kim SH, Park ZY, Song WK, et al. Interaction of SPIN90 with dynamin I and its participation in synaptic vesicle endocytosis. J Neurosci 2005;25(41):9515-9523.

38. Hinshaw JE. Dynamin and its role in membrane fission. Annu Rev Cell Dev Biol 2000;16:483-519.

39. Klein DE, Lee A, Frank DW, Marks MS, Lemmon MA. The pleckstrin homology domains of dynamin isoforms require oligomerization for high affinity phosphoinositide binding. J Biol Chem 1998;273(42):27725-27733.

40. Nakata T, Iwamoto A, Noda Y, Takemura R, Yoshikura H, Hirokawa N. Predominant and developmentally regulated expression of dynamin in neurons. Neuron 1991;7(3):461-469.

41. Shpetner HS, Vallee RB. Identification of dynamin, a novel mechanochemical enzyme that mediates interactions between microtubules. Cell 1989;59(3):421-432.

42. Altschuler Y, Barbas SM, Terlecky LJ, Tang K, Hardy S, Mostov KE, et al. Redundant and distinct functions for dynamin-1 and dynamin-2 isoforms. J Cell Biol 1998;143(7):1871-1881.

43. Damke H, Baba T, Warnock DE, Schmid SL. Induction of mutant dynamin specifically blocks endocytic coated vesicle formation. J Cell Biol 1994;127(4):915-934.

44. Gray NW, Fourgeaud L, Huang B, Chen J, Cao H, Oswald BJ, et al. Dynamin 3 is a component of the postsynapse, where it interacts with mGluR5 and Homer. Curr Biol: CB 2003;13(6):510-515.

45. Lundmark R, Carlsson SR. Sorting nexin 9 participates in clathrin-mediated endocytosis through interactions with the core components. J Biol Chem 2003;278(47):46772-46781.

46. Lundmark R, Carlsson SR. SNX9 - a prelude to vesicle release. J Cell Sci 2009;122(Pt 1):5-11.

47. Yarar D, Surka MC, Leonard MC, Schmid SL. SNX9 activities are regulated by multiple phosphoinositides through both PX and BAR domains. Traffic 2008;9(1):133-146.

48. Lundmark R, Carlsson SR. The beta-appendages of the four adaptor-protein (AP) complexes: structure and binding properties, and identification of sorting nexin 9 as an accessory protein to AP-2. Biochem J 2002;362(Pt 3):597-607.

49. Quan A, Robinson PJ. Rapid purification of native dynamin I and colorimetric GTPase assay. Methods Enzymol 2005;404:556-569.

50. Shin N, Lee S, Ahn N, Kim SA, Ahn SG, YongPark Z, et al. Sorting nexin 9 interacts with dynamin 1 and N-WASP and coordinates synaptic vesicle endocytosis. J Biol Chem 2007;282(39):28939-28950.

51. Lundmark R, Carlsson SR. Regulated membrane recruitment of dynamin-2 mediated by sorting nexin 9. J Biol Chem 2004;279(41):42694-42702.

52. Schobel S, Neumann S, Hertweck M, Dislich B, Kuhn PH, Kremmer E, et al. A novel sorting nexin modulates endocytic trafficking and alpha-secretase cleavage of the amyloid precursor protein. J Biol Chem 2008;283(21):14257-14268.

53. Heiseke A, Schobel S, Lichtenthaler SF, Vorberg I, Groschup MH, Kretzschmar H, et al. The novel sorting nexin SNX33 interferes with cellular PrP formation by modulation of PrP shedding. Traffic 2008;9(7):1116-1129.

54. Yarar D, Waterman-Storer CM, Schmid SL. SNX9 couples actin assembly to phosphoinositide signals and is required for membrane remodeling during endocytosis. Dev Cell 2007;13(1):43-56.

55. Lee VM, Goedert M, Trojanowski JQ. Neurodegenerative tauopathies. Annu Rev Neurosci 2001;24:1121-1159.

56. Lambert MP, Barlow AK, Chromy BA, Edwards C, Freed R, Liosatos M, et al. Diffusible, nonfibrillar ligands derived from Abeta1-42 are potent central nervous system neurotoxins. Proc Natl Acad Sci U S A 1998;95(11):6448-6453.

57. Walsh DM, Klyubin I, Fadeeva JV, Cullen WK, Anwyl R, Wolfe MS, et al. Naturally secreted oligomers of amyloid beta protein potently inhibit hippocampal long-term potentiation in vivo. Nature 2002;416(6880):535-539.

58. Haass C, Selkoe DJ. Soluble protein oligomers in neurodegeneration: lessons from the Alzheimer's amyloid beta-peptide. Nat Rev Mol Cell Biol 2007;8(2):101-112.

59. McLean CA, Cherny RA, Fraser FW, Fuller SJ, Smith MJ, Beyreuther K, et al. Soluble pool of Abeta amyloid as a determinant of severity of neurodegeneration in Alzheimer's disease. Ann Neurol 1999;46(6):860-866.

60. Demuro A, Mina E, Kayed R, Milton SC, Parker I, Glabe CG. Calcium dysregulation and membrane disruption as a ubiquitous neurotoxic mechanism of soluble amyloid oligomers. J Biol Chem 2005;280(17):17294-17300.

61. Snyder EM, Nong Y, Almeida CG, Paul S, Moran T, Choi EY, Nairn AC, et al. Regulation of NMDA receptor trafficking by amyloid-beta. Nat Neurosci 2005;8(8):1051-1058.

62. Hsieh H, Boehm J, Sato C, Iwatsubo T, Tomita T, Sisodia S, et al. AMPAR removal underlies Abeta-induced synaptic depression and dendritic spine loss. Neuron 2006;52(5):831-843.

63. Green KN, LaFerla FM. Linking calcium to Abeta and Alzheimer's disease. Neuron 2008;59(2):190-194.

64. Billings LM, Oddo S, Green KN, McGaugh JL, LaFerla FM. Intraneuronal Abeta causes the onset of early Alzheimer's disease-related cognitive deficits in transgenic mice. Neuron 2005;45(5):675-688.

65. Dodart JC, Bales KR, Gannon KS, Greene SJ, DeMattos RB, Mathis C, et al. Immunization reverses memory deficits without reducing brain Abeta burden in Alzheimer's disease model. Nat Neurosci 2002;5(5):452-457.

66. Kotilinek LA, Bacskai B, Westerman M, Kawarabayashi T, Younkin L, Hyman BT, et al. Reversible memory loss in a mouse transgenic model of Alzheimer's disease. J Neurosci 2002;22(15):6331-6335.

67. Abramov E, Dolev I, Fogel H, Ciccotosto GD, Ruff E, Slutsky I. Amyloid-beta as a positive endogenous regulator of release probability at hippocampal synapses. Nat Neurosci 2009;12(12):1567-1576.

68. Calabrese B, Shaked GM, Tabarean IV, Braga J, Koo EH, Halpain S. Rapid, concurrent alterations in pre- and postsynaptic structure induced by naturally-secreted amyloid-beta protein. Mol Cell Neurosci 2007;35(2):183-193.

69. Moreno H, Yu E, Pigino G, Hernandez AI, Kim N, Moreira JE, et al. Synaptic transmission block by presynaptic injection of oligomeric amyloid beta. Proc Natl Acad Sci U S A 2009;106(14):5901-5906.

70. Nimmrich V, Grimm C, Draguhn A, Barghorn S, Lehmann A, Schoemaker H, et al. Amyloid beta oligomers (A beta(1-42) globulomer) suppress spontaneous synaptic activity by inhibition of P/Q-type calcium currents. J Neurosci 2008;28(4):788-797.

71. Puzzo D, Privitera L, Leznik E, Fa M, Staniszewski A, Palmeri A, et al. Picomolar amyloid-beta positively modulates synaptic plasticity and memory in hippocampus. J Neurosci 2008;28(53):14537-14545.

72. Murthy VN, De Camilli P. Cell biology of the presynaptic terminal. Annu Rev Neurosci 2003;26:701-728.

73. Chang S, De Camilli P. Glutamate regulates actin-based motility in axonal filopodia. Nat Neurosci 2001;4(8):787-793.

74. Lee S, Lee K, Hwang S, Kim SH, Song WK, Park ZY, et al. SPIN90/WISH interacts with PSD-95 and regulates dendritic spinogenesis via an N-WASP-independent mechanism. EMBO J 2006;25(20):4983-4995.

75. Kim Y, Park J, Song WJ, Chang S. Overexpression of Dyrk1A causes the defects in synaptic vesicle endocytosis. Neurosignals 2010;18(3):164-172.

76. Granseth B, Odermatt B, Royle SJ, Lagnado L. Clathrin-mediated endocytosis is the dominant mechanism of vesicle retrieval at hippocampal synapses. Neuron 2006;51(6):773-786.

77. Schikorski T, Stevens CF. Morphological correlates of functionally defined synaptic vesicle populations. Nat Neurosci 2001;4(4):391-395.

78. Voglmaier SM, Kam K, Yang H, Fortin DL, Hua Z, Nicoll RA, et al. Distinct endocytic pathways control the rate and extent of synaptic vesicle protein recycling. Neuron 2006;51(1):71-84.

79. Burrone J, Li Z, Murthy VN. Studying vesicle cycling in presynaptic terminals using the genetically encoded probe synaptopHluorin. Nat Protoc 2006;1(6):2970-2978.

80. Zucker RS, Regehr WG. Short-term synaptic plasticity. Annu Rev Physiol 2002;64:355-405.

81. Lee SH, Kim KR, Ryu SY, Son S, Hong HS, Mook-Jung I, et al. Impaired short-term plasticity in mossy fiber synapses caused by

mitochondrial dysfunction of dentate granule cells is the earliest synaptic deficit in a mouse model of Alzheimer's disease. J Neurosci 2012;32(17):5953-5963.

82. Kim WT, Chang S, Daniell L, Cremona O, Di Paolo G, De Camilli P. Delayed reentry of recycling vesicles into the fusion-competent synaptic vesicle pool in synaptojanin 1 knockout mice. Proc Natl Acad Sci U S A 2002;99(26):17143-17148.

83. Wenk MR, Pellegrini L, Klenchin VA, Di Paolo G, Chang S, Daniell L, et al. PIP kinase Igamma is the major PI(4,5)P(2) synthesizing enzyme at the synapse. Neuron 2001;32(1):79-88.

84. Oakley H, Cole SL, Logan S, Maus E, Shao P, Craft J, et al. Intraneuronal beta-amyloid aggregates, neurodegeneration, and neuron loss in transgenic mice with five familial Alzheimer's disease mutations: potential factors in amyloid plaque formation. J Neurosci 2006;26(40):10129-10140.

85. Kim SH, Ryan TA. CDK5 serves as a major control point in neurotransmitter release. Neuron 2010;67(5):797-809.

86. Lee MS, Kwon YT, Li M, Peng J, Friedlander RM, Tsai LH. Neurotoxicity induces cleavage of p35 to p25 by calpain. Nature 2000;405(6784):360-364.

87. Qu J, Nakamura T, Cao G, Holland EA, McKercher SR, Lipton SA. S-Nitrosylation activates Cdk5 and contributes to synaptic spine loss induced by beta-amyloid peptide. Proc Natl Acad Sci U S A 2011;108(34):14330-14335.

88. Kelly BL, Ferreira A. Beta-amyloid disrupted synaptic vesicle endocytosis in cultured hippocampal neurons. Neuroscience 2007;147(1):60-70.

89. Patrick GN, Zukerberg L, Nikolic M, de la Monte S, Dikkes P, Tsai LH. Conversion of p35 to p25 deregulates Cdk5 activity and promotes neurodegeneration. Nature 1999;402(6762):615-622.

90. Celsi F, Svedberg M, Unger C, Cotman CW, Carri MT, Ottersen OP, et al. Beta-amyloid causes downregulation of calcineurin in neurons through induction of oxidative stress. Neurobiol Dis 2007;26(2):342-352.

91. Lauren J, Gimbel DA, Nygaard HB, Gilbert JW, Strittmatter SM. Cellular prion protein mediates impairment of synaptic plasticity by amyloid-beta oligomers. Nature 2009;457(7233):1128-1132.

Abstract in Korean (국문 초록)

SNX18 과 SNX9 은 같은 도메인 구조를 가진 SNXs family 인데, 지금까지 연구는 이들이 세포내 수송과정을 조절하는데 있어서 유사한 기능을 하는 것인지 서로 다른 기능을 하는 것인지에 관한 정확한 증거가 부족했다. 따라서 첫번째 장에서는 여러 실험을 통해 SNX18 이 세포내 수송과정에서 SNX9 과 다른 곳에서 다른 역할을 하는 것이 아니라 세포막 근처에 같이 위치하면서 SNX9 과 유사한 역할을 하고 있다는 것을 밝혀냈다. 즉, SNX18 은 대부분의 세포에서 비록 발현양은 다르지만 SNX9 과 같이 발현되고 있으며, dynamin 과 결합하여 이를 세포막으로 이동시킬 뿐 아니라 dynamin 의 GTPase activity 를 조절한다는 것을 증명하였다. 또한 N-WASP, synaptojanin 과 결합할 수 있으며, SNX9 과 SNX18 은 세포막의 tubule 구조에서 heterodimer 를 이루며 같이 위치한다는 것을 알게 되었다. SNX18-shRNA 를 넣어서 SNX18 의 발현을 막으면 transferrin uptake 가 방해되고, 이는 SNX9 을 과발현 시키면 다시 회복되는 것을 관찰하였다. 이러한 현상은 반대로 SNX9 발현이 저하되어 있는 세포에 SNX18 을 과발현 시켰을 경우에도 세포내 수송과정이 정상으로 회복되는 것을 관찰하였다. TIRF 현미경을 사용해서 SNX18 이 세포막에 있는 CCP 로 이동하는 것을 live cell 에서 관찰 할 수 있었으며, 이러한 이동은 dynamin 과 SNX9 의 이동과 시공간적으로 일치한다는 것을

밝혀냈다. 이러한 결과를 통해 본 논문에서는 SNX18 이 세포막에서 일어나는 세포내 수송과정에서 SNX9 과 함께 기능하며, 이들이 기능적으로 유사하게 작용함을 증명하였다.

지금까지의 실험이 신경세포가 아닌 일반세포에서 일어나는 세포내 수송과정에서 SNX18 의 역할에 대한 연구였다면, 두번째 장에서는 Aβ oligomers 가 신경세포에서 일어나는 세포내 수송과정, 시냅스낭의 순환과정에 어떤 영향을 미치는가에 관한 연구를 진행하였다. Aβ oligomers 는 알츠하이머병에 걸린 환자의 뇌에서 축적되어 있는 것으로 알려져 있는 물질로써, 알츠하이머병의 발병과 관련되어 있음이 잘 알려져 있다. 그러나 Aβ oligomers 가 시냅스 후세포의 기능장애에 미치는 영향에 관해서는 많은 연구가 집중되어 있는데 반해, 이것이 시냅스 전세포에 미치는 영향에 관한 연구는 미미하다. 따라서 두번째 장에서는 나노몰 농도의 Aβ oligomers 를 2 시간 처리한 후, 이것이 시냅스 전세포에서 일어나는 시냅스낭의 순환과정에 미치는 영향을 전반적으로 연구하였다. Aβ oligomers 를 처리한 신경세포의 시냅스낭의 구성 비율을 보면, recycling pool 이 작아지고 resting pool 이 증가한 것을 관찰할 수 있었으며, 전기자극이 주어지는 동안 일어나는 시냅스낭의 세포내 수송과정뿐 아니라 전기자극이 끝난 후에 일어나는 시냅스낭의 세포내 수송과정도 느려지는 것을 관찰할 수 있었다. 또한 세포막과

fusion 한 시냅스낭이 순환하여 다시 세포막과 fusion 하는데 걸리는 시간도 아무것도 처리안한 신경세포에 비해 Aβ oligomers 를 처리한 신경세포에서 현저히 느려진 것을 관찰할 수 있었다. 그러나 RRP 의 release probability 는 약간 증가하였고, RRP 를 depletion 시키는 자극을 준 후 10 초에서 80 초의 시간 간격을 두고 같은 자극을 주어 RRP 의 시냅스 낭이 회복되는 속도를 측정한 결과 이는 감소되어 있는 것을 관찰할 수 있었다. 그리고 이 모든 변화는 Aβ oligomers 와 결합하는 6E10 이라는 antibody 를 미리 Aβ oligomers 와 incubation 시킨 후 신경세포에 처리하면 나타나지 않음을 관찰하였다. 또한 Aβ oligomers 를 2 시간 처리하는 것만으로도 중요한 5-phosphatase 인 synaptojanin 의 발현양이 2-3 배 증가한 것을 관찰하였고, 칼슘이 제거되는 속도에는 변화가 일어나지 않음을 관찰하였다. 마지막으로 Aβ oligomers 에 의해 일어난 이러한 시냅스낭의 수송과정 변화의 원인을 연구한 결과, 시냅스낭의 비율이 변한 것은 Calpain inhibitor 를 미리 incubation 함으로써 회복되었으며, 세포내 수송과정이 느려진 것은 PIPkinase-γ 를 과발현시켜 PIP_2 발현을 증가시켰을때 완전히 정상으로 돌아옴을 관찰하였다. 그러나 PIPkinase-γ 를 과발현시킨 경우 Aβ oligomers 에 의해 변화한 시냅스낭의 비율은 정상으로 회복시키지 못했다. 이를 통해 Aβ oligomers 에 의해 일어나는 시냅스 전세포의 기능장애는 PIP_2 를

통한 과정과 Calpain-CDK5 를 통한 과정, 이렇게 두 가지 구별되는 downstream 이 있음을 밝혀냈다. 또한 이러한 결과를 통해 Aβ oligomers 가 두 개의 서로 다른 독립적인 downstream 과정을 통해 시냅스낭 수송과정의 여러 과정에 문제를 일으킴을 알게 되었으며, 이것이 알츠하이머병에서 나타나는 시냅스 기능장애를 일으킬 수 있음을 증명하였다.

주요어 : 세포내 수송과정, 세포막 함입, 전반사 형광현미경, 알츠하이머병, 아밀로이드 베타, 시냅스 기능장애, 시냅스낭 순환과정, 시냅스 전세포 기능

학 번 : 2009-30603